UNIVERSITAT POLITÈCNICA DE CATALUNYA
BARCELONATECH
Biomedical Engineering Research Centre

Programa de Doctorat en Enginyeria Biomèdica
Departament d'Enginyeria de Sistemes,
Automàtica i Informàtica Industrial
Centre de Recerca en Enginyeria Biomèdica

Tesis Doctoral por compendio de publicaciones

Muscular pattern based on multichanel surface EMG during voluntary contractions of the upper-limb

Mislav Jordanic

September 2017

Directores:
Miguel Angel Mañanas Villanueva
Mónica Rojas-Martínez

Abstract

Magnetoencephalography (MEG) is a noninvasive brain signal acquisition technique that provides excellent temporal resolution and a whole-head coverage allowing the spatial mapping of sources. These characteristics make MEG an appropriate technique to localize the epileptogenic zone (EZ) in the preoperative evaluation of refractory epilepsy.

Presurgical evaluation with MEG can guide the placement of intracranial EEG (iEEG), the current gold standard in the clinical practice, and even supply sufficient information for a surgical intervention without invasive recordings, reducing invasiveness, discomfort, and cost of the presurgical epilepsy diagnosis. However, MEG signals have low signal-to-noise ratio compared with iEEG and can sometimes be affected by noise that masks or distorts the brain activity. This may prevent the detection of interictal epileptiform discharges (IEDs) and high-frequency oscillations (HFOs), two important biomarkers used in the preoperative evaluation of epilepsy.

In this thesis, the reduction of two kinds of interference is aimed to improve the signal-to-noise ratio of MEG signals: metallic artifacts mask the activity of IEDs; and the high-frequency noise, that masks HFO activity. Considering the large number of MEG channels and the long duration of the recordings, reducing noise and marking events manually is a time-consuming task. The algorithms presented in this thesis provide automatic solutions aimed at the reduction of interferences and the detection of HFOs.

Firstly, a novel automatic BSS-based algorithm to reduce metallic interference is presented and validated using simulated and real MEG signals. Three methods are tested: AMUSE, a second-order BSS technique; and INFOMAX and FastICA, based on high-order statistics. The automatic detection algorithm exploits the known characteristics of metallic-related interferences. Results indicate that AMUSE performes better when recovering brain activity and allows an effective removal of artifactual components.

Secondly, the influence of metallic artifact filtering using the developed algorithm is evaluated in the source localization of IEDs in patients with refractory focal epilepsy. A comparison between the resulting positions of equivalent current dipoles (ECDs) produced by IEDs is performed: without removing metallic interference, rejecting only channels with large metallic artifacts, and after BSS-based reduction. The results show that a significant reduction on dispersion is achieved using the BSS-based reduction procedure, yielding feasible locations of ECDs in contrast to the other approaches.

Finally, an algorithm for the automatic detection of epileptic ripples in MEG using beamformer-based virtual sensors is developed. The automatic detection of ripples is performed using a two-stage approach. In the first step, beamforming is applied to the whole head to determine a region of interest. In the second step, the automatic detection of ripples is performed using the time-frequency characteristics of these oscillations. The performance of the algorithm is evaluated using simultaneous intracranial EEG recordings as gold standard.

The novel approaches developed in this thesis allow an improved noninvasive detection and localization of interictal epileptic biomarkers, which can help in the delimitation of the epileptogenic zone and guide the placement of intracranial electrodes, or even to determine these areas without additional invasive recordings. As a consequence of this improved detection, and given that interictal biomarkers are much more frequent and easy to record than ictal episodes, the presurgical evaluation process can be more comfortable for the patient and in a more economic way.

Resumen

La magnetoencefalografía (MEG) es una técnica no invasiva de adquisición de señales cerebrales que proporciona una excelente resolución temporal y una cobertura total de la cabeza, permitiendo el mapeo espacial de las fuentes cerebrales. Estas características hacen del MEG una técnica apropiada para localizar la zona epileptogénica (EZ) en la evaluación preoperatoria de la epilepsia refractaria.

La evaluación prequirúrgica con MEG puede orientar la colocación del EEG intracraneal (iEEG), el actual modelo de referencia en la práctica clínica, e incluso suministrar información suficiente para una intervención quirúrgica sin registros invasivos; reduciendo la invasividad, la incomodidad y el costo del diagnóstico de la epilepsia prequirúrgica. Sin embargo, las señales MEG tienen baja relación señal ruido en comparación con el iEEG pudiendo imposibilitar la detección de descargas epileptiformes interictales (IEDs) y oscilaciones de alta frecuencia (HFOs), dos importantes biomarcadores utilizados en la evaluación preoperatoria de la epilepsia.

En esta tesis, la reducción de dos tipos de interferencia está dirigida a mejorar la relación señal-ruido de la señal MEG: los artefactos metálicos que enmascaran la actividad de las IEDs; y el ruido de alta frecuencia, que enmascara la actividad de las HFOs. Debido al gran número de canales MEG y la larga duración de los registros, tanto reducir el ruido como seleccionar los biomarcadores manualmente es una tarea que consume mucho tiempo. Los algoritmos presentados en esta tesis aportan soluciones automáticas dirigidas a la reducción de interferencias y la detección de HFOs.

En primer lugar, se presenta y valida un nuevo algoritmo automático basado en BSS para reducir interferencias metálicas mediante señales simuladas y reales. Se prueban tres métodos: AMUSE, una técnica BSS de segundo orden; y INFOMAX y FastICA, basados en estadísticos de orden superior. El algoritmo de detección automático utiliza las características conocidas de la señal producida por la interferencia metálica. Los resultados indican que AMUSE recupera mejor la actividad cerebral y permite una eliminación efectiva de componentes artefactuales.

Posteriormente, se evalúa la influencia del filtrado de artefactos metálicos en la localización de IEDs en pacientes con epilepsia focal refractaria. Se realiza una comparación entre las posiciones resultantes de dipolos de corriente equivalentes (ECDs) producidos por IEDs: sin eliminar interferencias metálicas, rechazando solamente canales con elevados artefactos metálicos y, por último, después de una reducción utilizando el algoritmo BSS desarrollado. Los resultados

muestran que se logra una reducción significativa en la dispersión utilizando el procedimiento de reducción basado en BSS, lo que produce ubicaciones factibles de los dipolos en contraste con los otros enfoques.

En segundo lugar, se desarrolla un algoritmo para la detección automática ripples epilépticos en MEG utilizando sensores virtuales basados en la técnica de beamformer. La detección de ripples se realiza mediante un enfoque en dos etapas. Primero, se determina el área de interés usando beamformer. Posteriormente, se realiza la detección automática de ripples utilizando las características en tiempo-frecuencia. El rendimiento del algoritmo se evalúa utilizando registros iEEG simultáneos.

Los nuevos enfoques desarrollados en esta tesis permiten una detección no invasiva mejor de los biomarcadores interictales, que pueden ayudar a delimitar la zona epileptogénica y guiar la colocación de electrodos intracraneales, o incluso determinar estas áreas sin este tipo de registros. Como consecuencia de esta mejora en la detección, y dado que los biomarcadores interictales son mucho más frecuentes y fáciles de registrar que los episodios ictales, la evaluación prequirúrgica puede ser más cómoda y menos costosa para el paciente.

Contents

List of Tables

List of Figures

Chapter 1

Spatial distribution of HD-EMG improves identification of task and force in patients with incomplete spinal cord injury

Published as: Jordanić, M., Roja-Martínez, Mañanas, M.A., Alonso J.F. Spatial distribution of HD-EMG improves identification of task and force in patients with incomplete spinal cord injury *Journal of NeuroEngineering and Rehabilitation* 13(1):41, 2016

doi: 10.1186/s12984-016-0151-8

Impact Factor: 3.222; Position: 3 of 65 (Q1) REHABILITATION, 12 of 77 (Q1) BIOMEDICAL ENGINEERING.

Abstract: *Background.* Recent studies show that spatial distribution of High Density surface EMG maps (HD-EMG) improves the identification of tasks and their corresponding contraction levels. However, in patients with incomplete spinal cord injury (iSCI), some nerves that control muscles are damaged, leaving some muscle parts without an innervation. Therefore, HD-EMG maps in patients with iSCI are affected by the injury and they can be different for every patient. The objective of this study is to investigate the spatial distribution of intensity in HD-EMG recordings to distinguish co-activation patterns for different tasks and effort levels in patients with iSCI. These patterns are evaluated to be used for extraction of motion intention. *Method.* HD-EMG was recorded in patients during four isometric tasks of the forearm at three different effort levels. A linear discriminant classifier based on intensity and spatial features of HD-EMG maps of five upper-limb muscles was used to identify the attempted tasks. Task and force identification were evaluated for each patient individually, and the reliability of the identification was tested with respect to muscle fatigue and time interval between training and identification. *Results.* Three feature sets were analyzed in the identification: 1) intensity of the HD-EMG map, 2) intensity and center of gravity of HD-EMG maps and 3) intensity of a single differential EMG channel (gold standard). Results show that the combination of intensity and spatial features in classification identifies tasks and effort levels properly (Acc = 98.8%; S = 92.5%; P = 93.2%; SP = 99.4%) and outperforms significantly the other two feature sets ($p < 0.05$). *Conclusion.* In spite of the limited motor functionality, a specific co-activation pattern for each patient exists for both intensity, and spatial distribution of myoelectric activity. The spatial distribution is less sensitive than intensity to myoelectric changes that occur due to fatigue, and other time-dependent influences.

Keywords: Myoelectric control, Pattern recognition, High-density electromyography, Incomplete spinal cord injury

1.1 Backround

Surface electromyography (sEMG) is commonly used in noninvasive extraction of motor control information and identification of motion intention. Therefore, it has a wide practical application in rehabilitation engineering, e.g., prosthetics (Li et al., 2010; Young et al., 2013; Stango et al., 2015), exoskeletons (Vaca Benitez et al., 2013) and rehabilitation robots (Dipietro et al., 2005; Marchal-Crespo and Reinkensmeyer, 2009).

Conventional myocontrol is based on non-pattern recognition strategies. In a classical example of a single joint prosthesis (one degree of freedom), sEMG signals are recorded on two independent muscles. EMG of one muscle controls the intensity in one movement direction, and the EMG of another muscle in the opposite direction. The output force is proportional to EMG power of the controlling muscle. This strategy is simple, computationally efficient, robust, and does not need training, which makes it suitable for unsupervised, everyday use. However, it allows control only in one degree of freedom (DoF) at a time. Although this approach can provide intuitive interface with fewer commands (Hakonen et al., 2015), in case of a prosthetic device with multiple degrees of freedom (e.g. hand prostheses), switching between DoFs is impractical and requires a long time to complete a complex task (Farina et al., 2014).

On the other hand, pattern recognition-based control strategy enables usage of multiple DoFs without switching, which significantly improves task completion time (Hakonen et al., 2015). Although a variety of classifiers (e.g. hidden Markov model, support vector machine, artificial neural network, fuzzy logic) have been evaluated for task identification (Oskoei and Hu, 2007), multiple authors agree that the identification does not significantly depend on the classifier type (Hakonen et al., 2015; Hargrove et al., 2007; Zhang and Zhou, 2012). Therefore, simple and easy to train classifiers, e.g. linear discriminant analysis (LDA), are preferred (Scheme and Englehart, 2013; Boschmann and Platzner, 2013; Young et al., 2012; Li et al., 2014). Conversely, finding an appropriate set of features is challenging (Tkach et al., 2010; Liu and Zhou, 2013; **?**; Oskoei and Hu, 2006). Time-domain features are commonly used because they can achieve high identification results and are computationally efficient (Hakonen et al., 2015).

The technological advancement of EMG acquisition systems (Merletti et al., 2009; **?**) enables the use of high-density electromyography (HD-EMG). By using an array of closely spaced electrodes organized in a quadrature grid, a wide muscle area is recorded. This technology allows insights into the spatial distribution of the myoelectric intensity of a muscle. The spatial distribution allows monitoring the activation of different muscle regions, which depends on joint position (Vieira et al., 2010), contraction level (Holtermann et al., 2005), and duration of movement (Tucker et al., 2009). In addition, it has already been reported that spatial features can be used in task identification in normal subjects (Stango et al., 2015; Rojas-Martínez et al., 2013).

In patients with neurological disorders (e.g., stroke, spinal cord injury) motor control is impaired and some muscle parts can be left without innervation. As a result, patients often have problems with uncoordinated movements, lack of force, and spasticity. Rehabilitation and therapy can partially regenerate motor control, and either the affected muscles can recover partial functionality or other muscle groups can replace the functionality of a dysfunctional part. Therefore, the spatial distribution of motor unit action potentials is different from subject to subject and depends on the injury. But is it task-specific? And a more interesting question: is it force-specific? Liu & Zhou (Liu and Zhou, 2013) already proved that an intensity-related muscle co-activation pattern exists and that different hand tasks can be successfully identified in patients with incomplete spinal cord injury (iSCI). But can spatial distribution of myoelectric intensity help in identification of task and level of effort in patients with iSCI?

In this work, a method for the identification of different tasks and effort levels in patients with iSCI is proposed. High density EMG was measured on muscles participating in the analyzed contractions. By using different feature sets and an LDA classifier, we demonstrate that a specific co-activation pattern exists in patients with iSCI not only for a certain task, but also for a contraction intensity. Furthermore, the influence of time-dependent changes in EMG signal (due to muscle fatigue and drying of conductive gel) on the reliability of identification was evaluated. It was demonstrated that features related to spatial distribution not only improve the identification, but they are also more robust to time changes. What is more, they are helpful when identifying both the task and the desired force, indicating that spatial activation of motor units depends on type of exercise and contraction level in patients with iSCI.

1.2 Method

Measurements

Instrumentation

For the recording of HD-EMG signals, 2-D electrode arrays were fabricated in our laboratory (see Figure 1.1c). They were designed as silver-plated eyelets (5 mm external diameter), embedded in a hydrophobic fabric in a quadrature grid with 10 mm inter-electrode distance. When positioned and fixed with elastic straps, fabric follows the contour of the muscle enabling a constant electrical contact between subject's skin and eyelets.

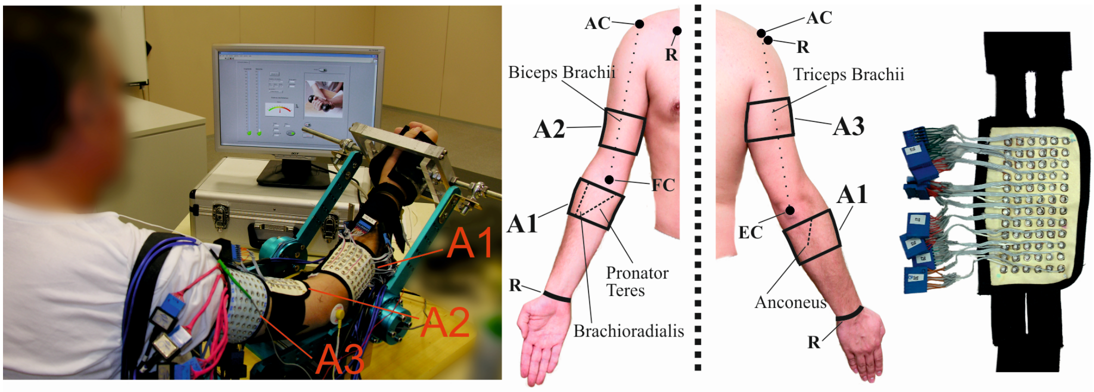

c) Experimental setup b) Electrodes location c) Electrode array

Figure 1.1: Experimental setup. **a)** Positioning of the electrode arrays A1-A3 during the recording. **b)** Anatomical landmarks and paths used for the positioning of the arrays: A1 (6 rows, 16 columns) was placed over the forearm covering Anconeus, Brachioradialis and Pronator Teres muscles, where the most proximal row of electrodes was placed 2 cm bellow the elbow crest (EC) covering all three muscles, according to (Kendall et al., 1993); A2 (6 rows, 12 columns) was placed in the distal part of the upper arm with respect to the center of the line connecting fossa cubit (FC) and acromion (AC), and covering Biceps Brachii muscle; A3 (6 rows, 12 columns) was placed in the proximal part with respect to the center of the line connecting EC and AC, over Triceps Brachii. Both A2 and A3 arrays were located in accordance with SENIAM recommendations Hermens and Freriks (1999). Reference electrodes (R) were placed on the clavicle, wrist and shoulder of the active arm. **c)** Detail of the electrode arrays used in the experiment

In total, 240 monopolar EMG channels were recorded for each patient using three electrode arrays. A "driven right leg" circuit (Merletti and Hermens, 2004) was used to reduce the common mode interference by feeding the common mode voltage with opposite phase to the patient.

Monopolar EMG signals were digitized using two amplifiers with synchronized sampling (EMG-USB- 128 channels, sampling frequency 2048 Hz, 3 dB bandwidth 10–750 Hz, programmable gains of 100, 200, 500, 1000, 2000, 5000, 10000, manufactured by LISiN-OT Bioelettronica).

In order to perform isometric contractions at the desired force, a mechanical brace was used and torque transducers (OT Bioelettronica, range 150 Nm, resolution 2.5 mV/V) were placed on each joint to record the exerted torque (Figure 1.1c). During the measurements, patients were sitting upright in front of the brace with their dominant arm immobilized at the wrist to avoid hand grip. The forearm was in the sagittal plane, halfway between pronation and supination. The elbow was flexed at 45° and the shoulder was adducted at 90° in the horizontal plane and flexed at 45° in the sagittal plane. The exerted force level was displayed online to patients during the exercise for visual feedback.

Experimental setup

Nine patients (four male, five female; age: 47 ± 18 years; body mass index: 28.2 ± 4.2) diagnosed with iSCI at C4-C6 levels participated in the study. Patients were rated C or D according to the ASIA scale and were injured at least 1 month before the experimental session. The study was conducted in accordance with the Declaration of Helsinki and subsequent amendments concerning research in humans and was approved by the Hospital Ethics Committee and the Local Government. All volunteers gave their written informed consent to participate.

HD-EMG was recorded during four isometric upper-limb tasks, i.e. flexion/extension of the elbow and supination/pronation of the forearm, on five superficial muscles involved by these tasks: Biceps Brachii, Triceps Brachii, Anconeus, Brachioradialis, and Pronator Teres. Prior to positioning of the electrode arrays, skin was cleaned, shaved, and treated with abrasive gel.

Three electrode arrays were used during the experiment: array A1 was placed over the forearm covering Anconeus, Brachioradialis and Pronator Teres muscles, and arrays A2 and A3 were placed over the upper arm covering Biceps Brachii and Triceps Brachii muscles. Reference electrodes were placed on the clavicle, wrist and shoulder of the active arm. After placing the arrays, each eyelet was filled with 20 μl of conductive gel using a gel dispenser (Multipette Plus, Eppendorf, Germany). The experimental setup can be seen in Figure 1.1.

HD-EMG recordings

Before signal recording, the maximal voluntary contraction (MVC) was measured for each task as a maximum of three consecutive trials. To prevent fatigue, each trial was followed by a three minute rest (Pizzigalli et al., 2014; Holobar et al., 2010). Patients were trained to keep their fingers and wrist relaxed in order to minimize the activity of forearm muscles that do not participate in the intended tasks.

The measurement protocol was composed of two parts. In the first part, contractions at three levels of effort (10%, 30% and 50% MVC) were measured for each task in randomized order. Visual feedback of the level of effort was provided in real time and subjects were asked to maintain the target level as precise as possible. Patients were instructed to remain at rest for three seconds followed by a contraction at a predefined force level for 10 s. There were three-minute breaks between consecutive recordings to prevent cumulative fatigue.

The second part of the measurement protocol began approximately half an hour (27.0 ± 9.8 min) after the end of the first part of the protocol. Each measurement started with a three-second rest period after which patients performed contraction at 50% MVC until failure. The procedure was repeated for each task and between recordings there were three-minute breaks. The recorded signals were divided into three sets for the subsequent analysis: the first set (submaximal set) was composed of the signals recorded in the first part of the protocol. The second set (time-effect set), used to test the time effect on the identification, was extracted from the beginning (up to 20% of the total duration of the contraction, TDC) of the signals recorded in the second part of the protocol. Finally, the third set (endurance set) was used to test the effect of myoelectric fatigue on the identification, and was composed of the totality of the signals recorded in the second part of the protocol. The flow chart of the recording protocol can be seen in Fig. 2.

HD-EMG maps and feature extraction

HD-EMG maps calculation

Low quality channels, a common issue in HD-EMG measurements, were identified by an expert system proposed by Rojas-Martínez et al. (Rojas-Martínez et al., 2012). The system is based on thresholds associated with the following three features: 1) relative power of low frequency components (from 0 to 12 Hz); 2) relative power of power-line components (50 Hz and first four harmonics); and 3) power calculated from RMS value of the signal. EMG channels without measurement artifacts were zero-phase filtered between 15 Hz and 350 Hz (Butterworth bandpass filter, 4^{th} order), and the first 6 harmonics of power line coupling were suppressed by using the adaptive transversal filter described in [30], whose weights were estimated by a least mean squares algorithm.

HD-EMG maps represent the spatial distribution of intensities of active motor units over the surface of the muscle:

$$HM_{i,j} = RMS\left(sEMG_{i,j}\right) \tag{1.1}$$

where HM is an activation map and each pixel in a map ($HM_{i,j}$) corresponds to an RMS value of a channel in an electrode array (position i, j). Maps were calculated on non-overlapping time windows of 250 ms to ensure an acceptable response time in applications directed to myoelectric control (Oskoei and Hu, 2007), and channels previously identified as artifacts were replaced by triangle-based cubic interpolation (Rojas-Martínez et al., 2012).

Feature extraction

Two types of features related to HD-EMG maps were extracted: intensity and center of gravity. They were used in classification individually or combined in order to compare their performance. Additionally, the intensity of a single differential channel, i.e. traditional bipolar recordings usually employed in pattern recognition as a "gold standard", was compared to other features. In any case, the feature set was composed of features extracted from all 5 monitored muscles. Multiple studies suggest that the relationship between EMG amplitude and generated force is not linear (Staudenmann et al., 2010; De Luca, 1997). Accordingly, the intensity features were calculated as a common logarithm of the mean intensity of the HD-EMG maps, which proved to achieve higher classification results than a linear measure (Rojas-Martínez et al., 2013):

$$I = \log_{10} \frac{1}{N} \sum_{i,j} HM_{i,j} \tag{1.2}$$

where I is an intensity feature calculated from the HD-EMG intensity map HM with a total number of N channels, and HM_{ij} is the intensity of a channel located at position i, j.

The center of gravity of an HD-EMG map (CG) was calculated as:

$$CG = \frac{1}{\sum_{i,j} HM_{i,j}} \sum_{i,j} HM_{i,j} \begin{bmatrix} i \\ j \end{bmatrix} \tag{1.3}$$

where (i, j) represents a channel position in the HD-EMG map HM.

The intensity of a single differential channel (Diff) was calculated as a common logarithm of an RMS value of difference of two consecutive channels in the direction of muscle fibers:

$$Diff = \log_{10} \Big(RMS \left(sEMG_{i,j} - sEMGi + 1, j \right) \Big) \tag{1.4}$$

where the locations of channels (i, j) and $(i + 1, j)$ are selected following SENIAM recommendations (Hermens and Freriks, 1999). Diff was calculated on the same 250 ms time epoch as the HD-EMG map.

Identification of motion intention

Classification

Three LDA classifiers based on different feature sets extracted from all five monitored muscles were evaluated in the study:

1. Classifier based on the intensity of the HD-EMG map (I)
2. Classifier based on the intensity and center of gravity of the HD-EMG map (I + CG)

3. Classifier based on the intensity of a single differential channel (gold standard) (Diff)

These classifiers were evaluated in the identification of task and level of contraction in patients with iSCI. Furthermore, the reliability of the classifiers was tested with respect to the slow time-dependent changes occurring in myoelectric signals, like those associated with gel drying or those related to changes at the physiological level (myoelectric fatigue).

Available observations were divided into a training group, which was used to train the classifier, and a validation group, which was used to evaluate classifier's performance. Both groups were balanced, i.e. there was an equal number of observations of each class in the training group, as well as in the validation group, and data were split into training and validation sets using a 50% / 50% ratio (Wang et al., 2015). To confirm the model was not overfitted, the results of classification of both sets were compared and were found similar. To achieve the statistical stability of results, each classifier was trained and evaluated in one thousand iterations, which are enough to avoid the potential error due to bad data partitioning (Zimmer and Sahle, 2016), and then classification results were averaged. In every iteration, observations in the training and validation groups were assigned randomly.

The performances of the classifiers were expressed in terms of accuracy (Acc), sensitivity (S), precision (P) and specificity (SP) (Farina et al., 2001), as described in the following equations:

$$Acc = \frac{TP + TN}{TP + FP + TN + FN} \tag{1.5}$$

$$S = \frac{TP}{TP + FN} \tag{1.6}$$

$$P = \frac{TP}{TP + FP} \tag{1.7}$$

$$SP = \frac{TN}{TN + FP} \tag{1.8}$$

where true positives (TP) is the number of samples correctly appended to a certain class; true negatives (TN) is the number of samples that do not belong to a certain class and were not classified to that class; false positives (FP) is the number of samples not belonging to a certain class, but wrongly classified into that class; and false negatives (FN) is the number of samples belonging to a certain class, but wrongly classified into another class.

Short-term identification

Classifiers with different sets of features (I, I + CG, and Diff) were tested on the submaximal set. Signals belonging to this set were recorded in a short time interval and, consequently, in the same conditions.

Two types of identification were considered: **1) Identification of tasks** and **2) Identification of tasks and effort levels**. Identification of tasks had 4 classes corresponding to the type of the task (flexion, extension, supination, and pronation) and an additional fifth class that corresponds to the rest period – no activity class (NoAct). Observations of no activity were extracted from the first three seconds of each recording, where subjects were asked to maintain at rest. Activity classes consisted of a mixture of all effort levels. On the other hand, identification of tasks and effort levels had 13 classes: 4 tasks with 3 levels of effort for each task (10% MVC, 30% MVC and 50% MVC) and NoAct class.

Considering that patients were not always able to maintain the target level of contraction given their condition, the torque signal was used to select only time segments where the measured force remained within a threshold of ±5%, ±10% and ±10% MVC for target contractions at 10%, 30% and 50% MVC. From every submaximal contraction 20 non-overlapping, 250 ms time epochs, closest to the target force were selected. This procedure ensured 20 observations for each task with differentiation on the level of effort, or 60 samples for each task, without differentiation on the effort level. Consequently, 60 observations without muscle activity were selected for NoAct class from the beginnings of exercises (rest period).

Influence of time- progress on identification

Wet electrodes with conductive electrolytic gel are commonly used for sEMG recording. However, these electrodes are not good for long-term monitoring (Searle and Kirkup, 2000). Gel drying increases skin-electrode impedance, affecting amplitude and spectral content of the recorded signal. Moreover, skin perspiration is enhanced under the electrode array, which also affects the skin-electrode impedance and, consequently, the characteristics of the recorded signal. To compare the performances of the different features, task identification was tested in these conditions.

Classifiers were trained on the submaximal set and validated on the time-effect contractions recorded in the second part of the protocol. As in the previous section, 20 time epochs for each task and level of effort were identified from the submaximal set based on the torque signal. Half the extracted observations of all levels of effort were used for training, following the recommendations of Scheme and Englehart (**?**), where it was noticed that a mixture of effort levels in the training group yields a more robust classifier. NoAct observations for the training group were extracted from recordings in the first part of the measurement protocol, whereas observations for the validation group were extracted from recordings in the second part of the protocol.

For comparison, the same classifier was used to validate contractions recorded at the first part of the protocol, i.e. using samples of the submaximal set. Since the classifier was trained on just half of the available observations from the submaximal set, the remaining observations were used for validation. But considering that time-effect set was composed of contractions recorded at 50% MVC effort level, the validation group was also composed only of 50% MVC contractions from the submaximal set.

The classifier was trained and evaluated over 1000 iterations with observations selected randomly both in the training and validation sets to avoid bias in the performance.

Influence of muscle fatigue on identification

Muscle fatigue is a slow change that occurs in contracting muscles. It alters the characteristics of recorded sEMG signal (i.e. amplitude and frequency content) (De Luca, 1984) and, inherently, alters the extracted classification features (Wan et al., 2010). To test the effect of fatigue on identification, each recording in the endurance set was divided into five equal time segments, i.e. 0–20% TDC, 20–40% TDC, 40–60% TDC, 60–80% TDC, and 80–100% TDC. The first segments (0–20% TDC) were used as a training group and the identification was carried out on all segments. The classification indices (accuracy, sensitivity, precision and specificity) were calculated for each segment in order to monitor performance during fatigue. The number of observations of each class was the same in the training group, as well as in the validation group.

Statistical methods

A repeated measures analysis of variance (ANOVA) was applied to the different performance indices using each type of task and effort level as measures and features used in the classification as factors. Both, within-subject and between-subject effects were considered in the analysis. In the case of endurance analysis, the repeated measures test was applied to account for differences attributed to the factor time, that is, duration of the contraction. In addition, differences between means were assessed through Student's t-test for paired samples. Effects and differences were considered significant at $p = 0.05$.

1.3 Results

1.3.1 Short-term identification

The different combinations of feature sets extracted from the five recorded muscles (l, I + CG, Diff) were evaluated in non-changing conditions, i.e. training and validation groups were extracted from the same contractions (submaximal set). Features were evaluated in 2 types of identification: 1) identification of tasks and 2) identification of tasks and effort levels.

The results of task identification are shown in Fig. 3. Adding spatial features to the classification improves the results and decreases the standard deviation. This is especially pronounced in sensitivity of flexion (88,8% ± 12,6% and 96,7% ± 5,5% in mean and standard deviation for I and I + CG features, respectively) and extension (89,6% ± 12,1% and 98,7% ± 2,0% for I and

I + CG features, respectively) as well as in precision of pronation (89,9% ± 12,5% and 96,6% ± 6,3% for I and I + CG features, respectively), and NoAct (85,6% ± 15,3% and 94,8% ± 6,5% for I and I + CG features, respectively). When evaluating differences in the performance of features through the repeated measures ANOVA, the within-subject effect was not significant when comparing indices obtained with the feature I or with the combination of features I + CG (either for accuracy, sensitivity, precision or specificity). However, the between subject effect was significant ($p < 0.05$ in all cases), showing that performance obtained for the combination of features I + CG was higher than that obtained when using the features I in the classification, independently of the evaluated task. Similar results were obtained when comparing performance of features Diff and I + CG: the within-subject effect showed no significant differences, that is, similar indices were obtained for all tasks (flexion, extension, supination, pronation and no activity), while the between-subjects effect was significant for all indices ($p < 0.05$) except for precision ($p = 0.07$), showing a higher performance for the features I + CG. No significant effects were observed when comparing the performance indices obtained with the features I with those obtained with the features Diff ($p.n.s.$).

Figure 4 shows the results of identification of tasks and effort levels. It can be noticed from the results that the identification based on intensity and spatial features displayed, in average, higher performance and lower standard deviation than the other two classifiers. Like in the previous case, the within-subject effect when comparing either between performance indices of I and I + CG or between performances of Diff and I + CG was not significant, showing similar results for all 13 classes (tasks and effort levels and no activity). However, the between-subjects effect was significant in both analyses ($p < 0.001$ when comparing I and I + CG; $p < 0.02$ when comparing Diff and I + CG), showing a higher performance for the case of the combination I + CG. Finally, when comparing performances between features I and Diff, no significant effects were observed ($p.n.s.$).

Figure 5 shows the performance of identification of tasks performed at a specific effort level. In this case, the classifier was trained using a mixture of all effort levels. The training group and the validation group were both extracted from the submaximal set. It can be noticed that all feature sets performed well when identifying tasks corresponding to high levels of contraction, but only the identification with spatial distribution maintained high performance and low standard deviation even at low contraction levels, i.e. 10% MVC, where paired t-tests showed that the identification based on intensity and spatial features significantly outperforms the other two types of features ($p < 0.04$).

1.3.2 Influence of time on identification

For the purpose of evaluation of the effect of time on identification, a classifier based on I + CG was trained using the submaximal set, and the identification was tested both on the submaximal set, and the time-effect set. Results are shown in Fig. 6, where it is possible to observe that the average performance significantly decreased with time (paired samples t-test showed $p < 0.05$) whereas the standard deviation increased.

Figure 7 shows performances of the different feature sets when the validation group was recorded after the training group, i.e. the classifier was trained on the submaximal set and recorded on the time-effect set. It can be noticed that the identification based on Diff features exhibited a significantly lower performance than the identifications based on I or I + CG features (paired samples t-test showed $p < 0.05$), while the identification based on I features performed similarly to the identification based on I + CG features (*p.n.s.*). This last can be understood in light of the results presented in the previous section, where the identification performances using these feature sets were similar at high-middle levels of effort, but I + CG outperformed I features at low effort levels (see Fig. 5).

1.3.3 Influence of time on identification

Figure 8 shows the influence of muscle fatigue on the identification based on intensity and center of gravity of the HD-EMG maps. It can be observed that average classification indices gradually decrease with fatigue. When evaluating differences in the performance of these indices, the within-subject effect given by the repeated measures analysis was significant ($p < 0,001$ in all indices). This result relies on the assumption of sphericity, that is, variances of the differences between all pairs of the repeated measurements should be equal; otherwise, result is positively biased. The conservative Greenhouse-Geisser correction method for the lack of sphericity (Greenhouse and Geisser, 1959) was applied to adjust the degrees of freedom (Landa and Everitt, 2004; Loftus and Masson, 1994) when the assumption of sphericity was violated. As suggested by Landa and Everitt (Landa and Everitt, 2004), Mauchly's test was used to test the sphericity.

Figures 9 and 10 display the influence of muscle fatigue on sensitivity and precision of the identification based on different feature sets. It can be noticed that all classifiers achieved high sensitivity and precision at the beginning of the endurance contractions, however, as the manifestations of myoelectric fatigue became more evident, the classifier based on intensity and spatial features outperformed the other two, both in average performance and variability.

1.4 Discussion

Nine subjects with iSCI performed four isometric forearm tasks (flexion, extension, supination, and pronation) at three levels of effort (10% MVC, 30% MVC, and 50% MVC). High density EMG was measured on five muscles of forearm and upper arm in monopolar configuration. Intensity maps were calculated for each muscle and three different feature sets were extracted: the average intensity of an HD-EMG map (I), the intensity and center of gravity of an HD-EMG maps (I + CG), and the intensity of a single differential channel (Diff) (gold standard). Using the extracted feature sets and LDA-based classification, both task and effort level were identified, and the influence of fatigue and other time-dependent changes (e.g. drying of conductive gel) on identification was evaluated. Since the goal of this study was to analyze different feature sets rather than classification methods, LDA was utilized given that this method is the most commonly used, and is generally recommended for myoelectric interfaces (Hakonen et al., 2015). Although it assumes normal distribution of patterns in each class, it has proven to have good performance even when the normality assumption does not hold (Grouven et al., 1996).

When identification using the different features was tested on signals recorded in short time intervals, the combination of I + CG outperformed the other feature sets. The results show that a muscular co-activation pattern exists not only for the task intention ($Acc = 98.7\%$; $S = 96.8\%$; $P = 97.0\%$; $SP = 99.2\%$), but also for the force intention ($Acc = 98.8\%$; $S = 92.5\%$; $P = 93.2\%$; $SP = 99.4\%$).

Although the identification based on the features Diff has slightly better performance in average than the identification based on the features I, a repeated measures ANOVA showed that there is no significant difference in their distributions. Moreover, a small displacement in the position of bipolar electrodes can have a great effect on signal intensity, as well as on spectral content. Consequently, if using Diff as features in classification, a small displacement can have a high influence on the identification performance. This effect does not exist in feature I, making it more robust to small changes in the position of the electrodes. On the other hand, the identification based on the combination of intensity and spatial features significantly outperforms both of them. This result was obtained both for identification of tasks and identification of tasks and effort levels. Furthermore, it has been shown that the classifier based on I + CG discriminates between types of tasks at low levels of effort (10% MVC) significantly better than the classifiers based on the other feature sets (Fig. 5).

The impedance between electrodes and skin changes during time on account of several causes, e.g., drying of conductive gel and sweating. Consequently, the identification performance deteriorates as the time between the training of the classifier and the identification increases. When the identification is performed long after the training of classifier, the results show that the identification based on I + CG performs just slightly better than the identification based on I features, while the identification based on Diff features is much worse ($S_{I+CG} = 94\%$, $P_{I+CG} = 95\%$; $S_I = 93\%$, $P_I = 94\%$; $S_{Diff} = 83\%$, $P_{Diff} = 83\%$). Although it may seem that, in average, spatial features do not improve the classification with respect to using only the intensity of an HD-EMG map, it is important to outline that these results were obtained on contractions of high levels of effort (50% MVC), where performances were similar even when contractions were recorded at the same time (see Fig. 5).

Muscle fatigue also affects the recorded EMG signal both in the time and spectral domains and therefore the identification performance deteriorates with fatigue. The results of this work show that the classifier based on intensity and spatial features is less sensitive to fatigue than classifiers based on the other feature sets. The proposed classifier shows a very good performance in task identification even at the final stage of fatigue ($Acc = 91.3\%$, $S = 84.3\%$, $P = 87.0\%$, $SP = 93.5\%$).

The proposed method could significantly improve the human-machine interface technology and can be used in numerous applications: computer games, exoskeletons, automatic wheelchairs, rehabilitation robots, prostheses, etc. As suggested by Müller-Putz et al. (Muller-Putz et al., 2015), non-invasive hybrid brain-computer interfaces (BCI) can be designed as EEG-based BCI supplemented with other biological and mechanical signals. For example, they reported significantly higher identification results for motion intention when using a hybrid BCI system composed of EEG and EMG sensory systems than when using only one of them. EMG usually has higher SNR ratio than EEG and it is widely used in the identification of the motion intention, however, it is prone to malfunction due to fatigue. When fatigue occurs, the supplemented EEG input keeps the identification stable, and increases the robustness of the system. Thus, advances in obtaining methods more robust to fatigue or time effect are very interesting.

Some patients with neuromuscular impairment can weakly activate their muscles, but insufficiently to generate a movement. In these patients, as well as in patients that can generate only weak movements, HD-EMG maps can be generated and used in identification of motion intention, as demonstrated in this study. This approach could supplement the existing BCI or inertial sensors based prostheses and result in a device with a better performance. For example, Rohm et al. (Rohm et al., 2013) performed a very interesting study with a single SCI patient. Their neuroprosthesis consisted of a functional electrical stimulation of the forearm and upper arm muscles, and a semiactive elbow orthosis. Using BCI and a shoulder joystick, the patient was able to perform complex hand and elbow tasks from everyday life (e.g. eating an ice cream cone). The reported performance of that study was 70%, which was remarkable considering the fact that the patient did not have any control over involved muscles. However, performance of similar patients could be increased using hybrid BCI if myoelectric activation exists.

Furthermore, compared to inertial signals, which are also used as input to control devices, EMG has a major advantage because myoelectric activation precedes the actual movement, which can save valuable response time.

However, it should be noted that although this study represents an improvement in the identification of motion intention, additional experiments should be considered in the future. Firstly, HD-EMG recordings were carried out during controlled isometric submaximal contractions, i.e.

patient's arm was fixed and supported by a mechanical brace. Since the methodology was capable to successfully and automatically differentiate between none, very low, low and medium effort levels, we might hypothesized that the method can be useful in prediction without the support of the brace. However, more experiments without the brace and the analysis of the recorded HD-EMG signals would be necessary to confirm and quantify this hypothesis.

1.5 Conclusion

In this study, the spatial distribution of EMG intensity was evaluated for identification of tasks and different levels of effort in patients with iSCI. Results show that the spatial activation of motor units is dependent on the type of exercise and contraction intensity, and that related features can improve identification performance.

Although results show that spatial features also enhance the robustness of the identification to time effect and fatigue, additional experiments need to be performed to test robustness to temporal dependent changes more thoroughly and to determine when the classifier fails by further tests done on fatigue.

The center of gravity was used as a figure of merit to describe the spatial distribution. Although it shows a significant improvement in classification, by definition it is insensitive to fine changes in the distribution of muscle units. Therefore, in future works, more appropriate measures of spatial distribution should be analyzed in order to better describe the spatial distribution of muscle intensity. Also, additional features as those related to the frequency content could be considered to improve even more the classification performance.

1.6 Declarations

1.6.1 Acknowledgements

We are grateful to Ursula Costa and Josep Medina as assistant and Head of the Functional Rehabilitation Service, respectively, of the Neurorehabilitation Hospital Institut Guttmann for their collaboration in the recruitment of patients and clinical support during the experiments carried out at the same Hospital.

This work has been partially supported by the Spanish Ministry of Economy and Competitiveness-Spain (project DPI2014-59049-R). MJ is supported by the grant for the recruitment of early-stage research staff (FI 2014) from the AGAUR, Generalitat de Catalunya, Spain.

1.6.2 Open Access

1.6.3 Competing interests

The authors declare that they have no competing interests.

1.6.4 Authors' contributions

MRM and MAM implemented the experimental protocol and conducted the experiments. MJ, MRM, and MAM designed the study and interpreted the results. MJ was in charge of the implementation of signal processing and machine learning methods and the analysis of the data. JFA aided in the analysis of the data and in the interpretation of results. All authors read and approved the final manuscript.

Chapter 2

Prediction of isometric motor tasks and effort levels based on high-density EMG in patients with incomplete spinal cord injury

Published as: Jordanić, M., Roja-Martínez, Mañanas, M.A., Alonso J.F. Prediction of isometric motor tasks and effort levels based on high-density EMG in patients with incomplete spinal cord injury *Journal of Neural Engineering* 13(4):46002, 2016

doi: 10.1088/1741-2560/13/4/046002

Impact Factor: 3.465; Position: 13 of 77 (Q1) BIOMEDICAL ENGINEERING, 90 of 258 (Q2) NEUROSCIENCES.

Abstract: *Objective.* The development of modern assistive and rehabilitation devices requires reliable and easy-to-use methods to extract neural information for control of devices. Group-specific pattern recognition identifiers are influenced by inter-subject variability. Based on high-density EMG (HD-EMG) maps, our research group has already shown that inter-subject muscle activation patterns exist in a population of healthy subjects. The aim of this paper is to analyze muscle activation patterns associated with four tasks (flexion/extension of the elbow, and supination/pronation of the forearm) at three different effort levels in a group of patients with incomplete Spinal Cord Injury (iSCI). *Approach.* Muscle activation patterns were evaluated by the automatic identification of these four isometric tasks along with the identification of levels of voluntary contractions. Two types of classifiers were considered in the identification: linear discriminant analysis and support vector machine. *Main results.* Results show that performance of classification increases when combining features extracted from intensity and spatial information of HD-EMG maps ($Accuracy$ = 97.5%). Moreover, when compared to a population with injuries at different levels, a lower variability between activation maps was obtained within a group of patients with similar injury suggesting stronger task-specific and effort-level-specific co-activation patterns, which enable better prediction results. *Significance.* Despite the challenge of identifying both the four tasks and the three effort levels in patients with iSCI, promising results were obtained which support the use of HD-EMG features for providing useful information regarding motion and force intention.

Keywords: Myoelectric control, pattern recognition, high-density electromyography, incomplete spinal cord injury

2.1 Introduction

Myoelectric signals have been extensively studied for more than half a century to understand muscle control strategies and to build rehabilitation and assistive devices. Surface electromyography (sEMG) is preferably used for monitoring because it is a non-invasive, easy-to-use method, rich in neural information, and has relatively high signal-to-noise ratio. It can be used in many and different applications: artificial limbs in prosthetics technology (Li et al., 2010; Huang et al., 2005), exoskeletons in assistive devices (Young et al., 2013), rehabilitation robots that stimulate neuroplasticity (Marchal-Crespo and Reinkensmeyer, 2009; Dipietro et al., 2005), and other human-machine interfaces.

Neuromuscular intention has lately often been identified using a pattern-recognition approach. Although many classifier types have been evaluated for the identification (support vector machine, k-nearest neighbor, hidden Markov models, artificial neural networks) (Oskoei and Hu, 2007), fast-to-train and computationally-efficient classifiers are preferable, e.g., linear discriminant analysis (Hakonen et al., 2015; Hargrove et al., 2007). On the other hand, the choice of features used in classification is very delicate. In literature, a lot of features have been considered in the time, frequency, and time-frequency domains as well as spatial features (Hakonen et al., 2015). Time domain features are commonly used because they are effective and easy to calculate (Hakonen et al., 2015).

Spatial features emerged with the appearance of high-density EMG systems (HD-EMG). Multiple EMG channels are recorded using a 2D array of closely spaced electrodes placed over the wide area of the muscle or group of muscles. This procedure allows the calculation of two-dimensional activation maps where the intensity of each pixel represents the intensity of a corresponding EMG channel. Consequently, the information on spatial distribution of EMG intensity over the muscle is provided. Recent studies show that changes in the spatial activation pattern are related to the duration of movement and fatigue (Tucker et al., 2009; Staudenmann et al., 2014), the position of the joint (Vieira et al., 2010) and the level of contraction (Holtermann et al., 2005). Since the spatial distribution contains a lot of information about the muscle, it is acknowledged as a valuable feature in the identification of motion intention (Hakonen et al., 2015; Stango et al., 2015; Rojas-Martínez et al., 2013).

Most pattern-recognition identification methods are subject-specific. This could be avoided by building a single identifier for a group of patients, i.e. group-specific identifier. However, inter-subject variability is a big concern when designing a group-specific pattern recognition-based identifier. Individuals differ from each other when referring to physiological parameters, e.g., conductivity of subcutaneous tissue and limb dimension. Nevertheless, by comparing HD-EMG activation maps, inter-subject activation patterns for different tasks and levels of contraction were demonstrated to exist in a population of healthy subjects (Rojas-Martínez et al., 2012). Furthermore, by using intensity and spatial features extracted from activation maps it is possible to construct an inter-subject identification method not only for different tasks, but also for different effort levels (Rojas-Martínez et al., 2013). The authors also reported that in healthy subjects the performance improved by adding spatial features in the identification, proving that spatial distribution is less sensitive to inter-subject variability.

Unfortunately, in patients with incomplete spinal cord injury (iSCI) and other neurological disorders (e.g. stroke), motor control is impaired as a result of damaged nerves. Patients can have uncoordinated movements and lack of force, or, in more difficult cases, they can weakly activate their muscles, but cannot perform the movement. If motion intention could be extracted from muscle activity, that is, EMG, in real time, it would allow them to control external devices even without kinematic sensors. This technology could be helpful during therapy (e.g., Hogan et al. (Hogan et al., 2006) reported that robotic rehabilitation can be improved by patients' active participation), as well as in everyday life after the injury by using exoskeleton systems. It has already been shown that intensity-related and task-specific activation patterns exist in patients with neuromuscular impairment and that motion intention can be extracted; e.g. using time domain and autoregressive model features Liu and Zhou (Liu and Zhou, 2013) were able to perform patient-specific identification of tasks with high performance in patients with iSCI, Zhang and Zhou (Zhang and Zhou, 2012) in stroke patients, whereas Geng et al. (Geng et al., 2014) in mildly-impaired traumatic brain injury patients. However, all of these studies considered subject-specific patterns, that is, the identification was trained and validated individually for each subject in the databases.

To our best knowledge, no studies have evaluated group-specific identification of motion intention in patients with iSCI so far. It is a particularly difficult task because of the diverse nature of injuries among patients, which can result in high variability among activation maps. The objective of this study is twofold: firstly, to analyze patterns in the activation maps associated with four movement directions at the elbow joint and with different strengths in a group of patients with iSCI; and secondly, the automatic identification of these four isometric tasks and the differentiation between levels of voluntary contraction at low-medium efforts. For this purpose, HD-EMG was recorded on patients with iSCI while performing the following motor tasks: flexion, extension, supination and pronation of the forearm at three different effort levels. HD-EMG activation maps were calculated and variability was measured between maps of different patients. Furthermore, inter-subject identification of tasks and effort levels was performed using intensity and spatial features calculated from activation maps.

2.2 Methodololgy

Experimental Protocol

Nine patients (age: 45 ± 20 years; body mass index: 27.1 ± 5.2; five male and four female) participated in the experiment. They were all diagnosed with incomplete spinal cord injury (rated C or D according to ASIA scale) and they were injured at least 1 month before the experiment. There were six patients with injury at C4 vertebra and three patients with injuries at C3, C5 and C6 vertebras. The study was approved by the local ethics committee and all patients gave their written consent. Subjects performed four isometric upper-limb tasks following the same experimental protocol carried out in [14]: flexion and extension at the elbow and supination and pronation of the forearm. High-density EMG was recorded on five superficial muscles of the upper-arm and forearm, which are dominantly involved in these tasks: Biceps Brachii, Triceps Brachii, Brachioradialis, Anconeus and Pronator Teres.

During the experiments, patients were sitting upright in front of a table with their dominant arm fixed using a mechanical brace to perform isometric contractions at the elbow (Figure 1). The forearm was in the sagittal plane, halfway between pronation and supination. The elbow was flexed at 45° and the shoulder was adducted at 90° in the horizontal plane and flexed at 45° in the sagittal plane. Two torque transducers (OT Bioelettronica, range 150 Nm, resolution 2.5 mV/V) were installed in the brace to measure the force exerted at the elbow, which was displayed to patients during the exercise as visual feedback. HD-EMG monopolar signals were recorded using electrode arrays manufactured in our laboratory. They were designed as silver-plated eyelets (5 mm external diameter) embedded in hydrophobic, non-conductive fabric in a 10 mm × 10 mm quadrature grid. Elastic straps were used to fix the arrays to the patient's skin. Three electrode arrays were used to gather a total of 240 monopolar EMG signals for each patient. The first array (6 rows × 16 columns) was used to record HD-EMG of forearm muscles (Brachioradialis, Anconeus and Pronator Teres) and was placed so that the most proximal row of electrodes was 2 cm below the elbow crease. The locations of the muscles were previously marked on the skin surface according to (Kendall et al., 1993) and the array was placed to cover all three of them. The second and third array (6 rows × 12 columns each) were placed following the recommendations of the SENIAM project (Hermens and Freriks, 1999) and they covered the

Biceps Brachii (distal part of the upper-arm) and Triceps Brachii (proximal part of the upper-arm) respectively. The reference electrodes were placed on the clavicle, wrist, and shoulder of the active arm. When placed, each eyelet was filled with 20 μl of conductive gel using a gel dispenser (Multipette Plus, Eppendorf, Germany). Signals were recorded using two commercial EMG amplifiers with synchronized sampling (EMG-USB- 128 channels, sampling frequency 2048 Hz, 12-bit A/D converter, 3 dB bandwidth 10-750 Hz, programmable gains of 100, 200, 500, 1000, 2000, 5000, 10000, manufactured by LISiN-OT Bioelettronica). At the beginning of the experimental protocol, the maximal voluntary contraction (MVC) was measured for each task, obtained as the maximum of three consecutive trials. Between each trial there was a three minute rest to prevent cumulative fatigue. Afterwards, submaximal contractions for the four tasks at three different levels of effort (10% MVC, 30% MVC and 50% MVC) were measured. Patients were asked to maintain the target force as precisely as possible for 10 seconds while the exerted level was displayed to them. Recordings were performed in randomized order and between consecutive recordings there were three minute breaks to prevent muscle fatigue.

HD-EMG Activation Maps

In order to increase *signal-to-noise ratio* (SNR), the obtained HD-EMG signals were zero-phase filtered between 15 Hz and 350 Hz using a Butterworth band-pass filter of 4^{th} order. Additionally, the power line interference was suppressed using the adaptive filter described in (Mañanas et al., 2001). Channels containing measurement artifacts were identified and removed following the procedure described in (Rojas-Martínez et al., 2012). Based on the torque measurements, 20 time epochs of 250 ms were selected for every recording during which patients were able to maintain the torque level within a range of $\pm 5\%$, $\pm 7.5\%$, and $\pm 10\%$ MVC for the targets of 10%, 30%, and 50% MVC respectively. On the selected epochs, HD-EMG maps, HM, were calculated as:

$$HM_{i,j} = \sqrt{\frac{1}{N}\sum_{n=0}^{N-1} sEMG^2_{i,j}[n]} \tag{2.1}$$

where HM was calculated for $N = 512$ samples corresponding to 250 ms. Maps were calculated as the RMS values obtained from myoelectric signals ($sEMG$), where the position (i, j) of a channel in the array was equivalent to the position of a pixel in the map. Channels identified as artifacts were substituted using a triangular-based cubic interpolation (Rojas-Martínez et al., 2012).

To reduce crosstalk activity of adjacent muscles that can occur on the borders of the map, maps were segmented according to (Rojas-Martínez et al., 2012). This procedure ensured that maps were localized and represented only regions of the associated muscle activity.

To calculate comparable activation maps among patients, spatial coordinates were normalized with respect to limb dimensions and position of an electrode array for every patient. A coordinate system was built for each muscle where the x-axis was parallel to the medial-lateral direction, whereas the y-axis was parallel to the proximal-distal direction. The x-axis was normalized with respect to the upper-arm circumference measured at the muscle belly of either Biceps Brachii or Triceps Brachii for their corresponding maps, and with respect to the forearm circumference measured at the muscle belly of Brachioradialis for all three forearm muscle maps (Brachioradialis, Anconeus and Pronator Teres). Similarly, the y axis was normalized with respect to the distance between the Acromion and the Fossa Cubit for Biceps Brachii, the distance between the Acromion and the Olecranon for Triceps Brachii map and the distance between the medial Epicondyle and the Apofisis of the Radius for forearm muscles (Brachioradialis, Anconeus and Pronator Teres).

The origins of these coordinate systems for muscles of upper-arm were set following SENIAM recommendations (Hermens and Freriks, 1999), that is, the point located at 3/4 of the distance between Acromion and the Fossa Cubit for Biceps Brachii and 1/2 of the distance between Acromion and the Olecranon for Triceps Brachii. The origin of the coordinate system for each muscle of the forearm was located on the line that connects the origin and insertion of the muscle (Kendall et al., 1993) 2 cm bellow the elbow crease.

Representative activation maps for each patient and recording were obtained by averaging 20 activation maps HM (Eq. 2.1). These maps were then averaged between individuals to obtain activation maps for the group of patients. Since tissue conductivity and electrode-skin impedance is different from patient to patient, the recorded sEMG amplitude can vary a lot between patients. To compensate this effect, the dispersion of each pixel was expressed in terms of relative standard deviation (RSD), i.e. standard deviation between representative maps of different patients was calculated for each pixel in the map, and was then divided by the intensity value of the corresponding pixel in the average activation map. Finally, the average RSD of a map was calculated as the mean value of RSD of all pixels in a map.

Identification

Two types of classifiers were evaluated: linear discriminant analysis (LDA), and support vector machine (SVM) with a radial kernel. Classification was performed in MATLAB (version 2015a) using the Statistics and Machine Learning Toolbox (mat). Although when using LDA it is assumed that the patterns in each class are multivariate normally distributed with different means and identical covariance matrices, it is shown to be robust against deviations from the multivariate normality assumption (Grouven et al., 1996).

The features used in identification were the intensity and the center of gravity of HD-EMG maps calculated over 250 ms epochs.

Intensity was calculated as the common logarithm of the mean intensity of the map:

$$I = \log_{10} \frac{1}{N} \sum_{i,j} HM_{i,j} \tag{2.2}$$

where I is the intensity feature calculated for an $N-$ channel HD-EMG map (HM). The center of gravity was calculated as:

$$CG = \frac{1}{\sum_{i,j} HM_{i,j}} \sum_{i,j} HM_{i,j} \begin{bmatrix} i \\ j \end{bmatrix} \tag{2.3}$$

where CG is the center of gravity of the HD-EMG map HM, and (i,j) represents position of the channel in the map.

Two types of identification were performed: **1) identification of tasks** and **2) identification of tasks and effort levels**. In identification of tasks, four types of contraction were identified:

flexion, extension, supination and pronation. Performances were compared between using only intensity features and using the combination of intensity and spatial features of all five monitored muscles. In this sense, the possible improvement of pattern recognition was evaluated when adding spatial information.

A conjoint identification of tasks and effort levels was constructed as classification in two steps (Rojas-Martínez et al., 2013) (Figure 2). In the first step, the identification of tasks was performed, while in the second step, the level of effort of the identified task was determined. The second step was organized as 4 different classifiers, i.e. a single classifier for the identification of the effort level for each task (Figure 2). The features used in the identification of level of effort were the intensity and the center of gravity of the agonist-antagonist muscle pair involved in the task (Rojas-Martínez et al., 2013): Biceps Brachii and Triceps Brachii both for flexion and extension, Biceps Brachii, Brachioradialis and Anconeus for supination, and Pronator Teres and Anconeus for pronation. Two different approaches were used: the identification of three effort levels (10% MVC, 30% MVC, and 50% MVC) and the identification of two effort levels (low, corresponding to 10% MVC, and moderate, corresponding to 30% and 50% MVC). Thus, a total of 12 different classes for the first approach and 8 classes for the second were considered, and accordingly, a confusion matrix of 12 or 8 classes was formed at the output of the second step of the classifier for the evaluation of the identification. Therefore, if a task was misclassified in the first step but the level of effort was correctly classified in the second step, this observation counted as a misclassification.

Observations from all patients were pooled together and the identification was tested using the holdout method where 60% of the data were used for training and 40% for validation. Results were expressed in terms of accuracy (Acc), sensitivity (S), precision (P), and specificity (SP) (Farina et al., 2001):

$$Acc = \frac{TP + TN}{TP + FP + TN + FN} \tag{2.4}$$

$$S = \frac{TP}{TP + FN} \tag{2.5}$$

$$P = \frac{TP}{TP + FP} \tag{2.6}$$

$$SP = \frac{TN}{TN + FP} \tag{2.7}$$

where TP (true positive) is the number of samples belonging to a certain class and classified to that class, TN (true negative) is the number of samples not belonging to a certain class and not classified to that class, FP (false positive) is the number of samples not belonging to a certain class and classified to that class, and FN is the number of samples belonging to a certain class and classified to another class.

To reduce bias, a repeated holdout testing method was performed, i.e. the identification results were averaged over 20 iterations with randomized grouping for training and validation sets.

2.3 Results

2.3.1 Activation Maps

Activation maps were calculated and averaged among patients to obtain general activation maps for tasks and levels of effort in order to observe the activation pattern of the muscles.

Table 2.1 presents the relative standard deviation (RSD) between representative activation maps of individual patients. Results are shown for all patients in the database and also only for patients injured at the C4 level. It can be seen that the variability of the group increased notably when patients with injury different to C4 were included. Thus, patients with the C4 level of injury can be considered as a homogenous group.

The activation maps averaged among patients with lesion at the C4 level are displayed in Figure 3. The maps were interpolated by factor 20 in both directions and cropped to the active regions for display purposes only. In addition, the spatial distribution of RSD for the same group of patients and for the same level of effort is shown in Figure 4. It can be seen that RSD was lower for Biceps Brachii and Triceps Brachii during their main tasks (flexion and extension,

Table 2.1: Relative standard deviation of activation maps for each muscle and effort level averaged between the group of all patients (top) and group of patients with C4 level of injury (bottom).

Group of all patients

	10% MVC	30% MVC	50% MVC	All effort levels
Biceps	49.7%	54.6%	57.3%	53.9%
Triceps	65.4%	65.5%	64.5%	65.1%
Brachioradialis	59.9%	67.6%	67.1%	64.9%
Anconeus	39.0%	40.6%	40.7%	40.1%
Pronator Teres	54.2%	58.3%	57.6%	56.7%
Average	**53.6%**	**57.3%**	**57.4%**	**56.1%**

Group of patients with C4 level of injury

	10% MVC	30% MVC	50% MVC	All effort levels
Biceps	38.1%	39.9%	41.7%	39.9%
Triceps	48.7%	47.2%	50.1%	48.6%
Brachioradialis	25.5%	28.1%	31.1%	28.2%
Anconeus	32.9%	32.9%	35.8%	33.9%
Pronator Teres	35.6%	36.1%	35.5%	35.7%
Average	**36.2%**	**36.8%**	**38.8%**	**37.3%**

respectively) indicating that patients had similar activation patterns. On the other hand, the RSD for these muscles was higher during supination and pronation, which indicates different activation strategies among patients. The inter-subject variability was lower for the forearm muscles, especially the Anconeus.

Table 2.2 shows the percentages of the areas of the activation maps used to calculate the features.

Table 2.2: Percentages of the activation maps covered by the electrode arrays in each patient. Results are presented for each muscle as mean and standard deviation within the group of all patients (top) and group of patients with C4 level of injury (bottom).

Group of all patients

Biceps	Triceps	Brachioradialis	Anconeus	Pronator Teres
50% ± 7%	42% ± 7%	36% ± 8%	25% ± 9%	37% ± 12%

Group of patients with C4 level of injury

Biceps	Triceps	Brachioradialis	Anconeus	Pronator Teres
48% ± 8%	42% ± 8%	35% ± 5%	22% ± 8%	36% ± 13%

2.3.2 Identification of Tasks

Firstly, the influence of the effort level in the task identification was evaluated. The performance is shown in Figures 5 to 8 using the LDA classifier while both training and validation sets were composed of recordings at a specific effort level (10%, 30%, or 50% MVC). The task identification improved considerably when adding CG to the intensity features for the classification in both groups: all patients (Figure 5 with respect to Figure 7) and patients with C4 level of injury (Figure 6 with respect to Figure 8). In addition, when comparing between the two groups, the identification performance was better in the latter (Figures 5 and 7 compared to Figures 6 and 8, respectively). These improvements were observed at all the effort levels. However, when comparing between effort levels, the performance indices (especially sensitivity and precision) were lower at 10% MVC than at 30% or 50% MVC, particularly when combining intensity with spatial features (Figures 7 and 8). This points out to a lower reliability when identifying tasks at very low levels of contraction.

Secondly, the task identification (flexion, extension, supination and extension) based on different sets of features was performed on the pooled data of all three effort levels, using the LDA (Table 2.3) and the SVM (Table 2.4) classifiers. It is shown again that the results for task identification when using the LDA classifier are higher for the group of patients with a C4 level of injury than for the group of patients with all levels of injury. Although this could be noticed from the performance indices when only the intensity features were used (ΔAcc = 4.1%; ΔS = 8.2%; ΔP = 7.8%; ΔSP = 2.7%), it was more pronounced when spatial features were added to the identification, especially regarding sensitivity and precision (ΔAcc = 7.6%; ΔS = 15.2%; ΔP = 15.2%; ΔSP = 5.1%). The observed differences between groups could be explained by a lower relative standard deviation between activation maps of patients with C4 level of injury than between maps of all patients). These differences between groups in the automatic identification were removed when using a non-linear classifier, that is, a radial kernel SVM, whose separation power is greater than the higher dispersion of activation maps when the complete group was considered.

On the other hand, the performance of both classifiers improved when the center of gravity was added to the intensity features in the classification (ΔAcc = 7.2%; ΔS = 14.5%; ΔP = 14.3%;

Table 2.3: Identification of tasks using LDA classifier

	Intensity features			
	Accuracy	**Sensitivity**	**Precision**	**Specificity**
Flexion	82.6% ± 1.2%	61.9% ± 3.3%	66.3% ± 2.7%	89.5% ± 1.0%
Extension	79.2% ± 1.1%	62.6% ± 4.5%	57.9% ± 2.1%	84.8% ± 1.4%
Supination	82.8% ± 1.1%	61.5% ± 3.4%	67.0% ± 2.7%	89.9% ± 1.1%
Pronation	79.7% ± 1.1%	62.6% ± 2.5%	58.9% ± 2.6%	85.4% ± 1.8%
AVG all patients	**81.1% ± 1.1%**	**62.1% ± 3.4%**	**62.5% ± 2.5%**	**87.4% ± 1.3%**
AVG C4	**85.2% ± 1.0%**	**70.3% ± 3.4%**	**70.3% ± 2.6%**	**90.1% ± 1.4%**

	Combination of Intensity and center of gravity features			
	Accuracy	**Sensitivity**	**Precision**	**Specificity**
Flexion	90.7% ± 0.8%	83.3% ± 2.1%	80.4% ± 2.3%	93.2% ± 1.1%
Extension	84.6% ± 1.1%	73.3% ± 2.9%	67.8% ± 2.8%	88.3% ± 1.7%
Supination	91.6% ± 0.9%	84.3% ± 2.5%	82.6% ± 1.9%	94.1% ± 0.7%
Pronation	86.2% ± 1.0%	65.4% ± 2.6%	76.2% ± 2.9%	93.1% ± 1.1%
AVG all patients	**88.3% ± 0.9%**	**76.6% ± 2.5%**	**76.8% ± 2.5%**	**92.2% ± 1.2%**
AVG C4	**95.9% ± 0.9%**	**91.8% ± 2.3%**	**92.0% ± 2.1%**	**97.3% ± 0.8%**

Table 2.4: Identification of tasks using SVM classifier

	Intensity features			
	Accuracy	**Sensitivity**	**Precision**	**Specificity**
Flexion	95.9% ± 0.6%	89.8% ± 1.6%	93.8% ± 1.8%	98.0% ± 0.6%
Extension	95.8% ± 0.9%	93.2% ± 3.0%	90.4% ± 1.7%	96.7% ± 0.6%
Supination	95.9% ± 0.6%	90.3% ± 2.0%	93.2% ± 1.9%	97.8% ± 0.6%
Pronation	95.4% ± 0.8%	92.8% ± 1.6%	89.3% ± 2.6%	96.3% ± 1.1%
AVG all patients	**95.8% ± 0.7%**	**91.5% ± 2.0%**	**91.7% ± 2.0%**	**97.2% ± 0.7%**
AVG C4	**95.9% ± 0.7%**	**91.8% ± 2.5%**	**91.9% ± 2.4%**	**97.3% ± 0.9%**

	Combination of Intensity and center of gravity features			
	Accuracy	**Sensitivity**	**Precision**	**Specificity**
Flexion	98.8% ± 0.4%	97.2% ± 0.9%	97.8% ± 1.0%	99.3% ± 0.3%
Extension	99.0% ± 0.4%	98.1% ± 1.0%	98.0% ± 0.9%	99.3% ± 0.3%
Supination	98.7% ± 0.4%	98.1% ± 0.8%	96.8% ± 1.0%	98.9% ± 0.4%
Pronation	99.4% ± 0.3%	98.4% ± 1.0%	99.2% ± 0.4%	99.7% ± 0.1%
AVG all patients	**99.0% ± 0.4%**	**97.9% ± 0.9%**	**98.0% ± 0.8%**	**99.3% ± 0.3%**
AVG C4	**99.1% ± 0.4%**	**98.2% ± 1.2%**	**98.2% ± 1.0%**	**99.4% ± 0.4%**

$\Delta SP = 4.8\%$ for LDA; $\Delta Acc = 3.2\%$; $\Delta S = 6.4\%$; $\Delta P = 6.3\%$; $\Delta SP = 2.1\%$ for SVM). For this reason, the results for the conjoint identification of tasks and effort levels are presented only for the combination of intensity and spatial features in the next Section.

Finally, when comparing the two classifiers, the results showed that the SVM notably outperformed the LDA for both combinations of features ($\Delta Acc = 14.7\%$; $\Delta S = 29.4\%$; $\Delta P = 29.2\%$; $\Delta SP = 9.8\%$ when using only intensity features; and $\Delta Acc = 10.7\%$; $\Delta S = 21.4\%$; $\Delta P = 21.2\%$; $\Delta SP = 7.1\%$ when using the combination of both intensity and center of gravity features).

2.3.3 Identification of Tasks and Effort Levels

The performance indices for conjoint identification of the four tasks and the three effort levels using intensity and spatial features are presented in Table 2.5 and Table 2.7 for the LDA and SVM classifiers, respectively. Analogously, the joint identification of the four tasks and low and moderate effort levels are presented in Table 2.6 and Table 2.8 for the LDA and the SVM classifiers, respectively. Similarly to the task identification, improvements considering the group of patients with a C4 level of injury with respect to the whole group were found when using the LDA, but not with the SVM classifier ($\Delta Acc = 3.8\%$; $\Delta S = 22.6\%$; $\Delta P = 23.6\%$; $\Delta SP = 2.1\%$ for identification of three levels of effort; $\Delta Acc = 5.8\%$; $\Delta S = 23.1\%$; $\Delta P = 23.4\%$; $\Delta SP = 3.3\%$ for identification of low and moderate effort levels).

Both in the LDA and SVM classifiers the improvement could be seen when identifying low and moderate effort levels instead of three contraction levels ($\Delta S = 14.3\%$; $\Delta P = 15.9\%$ for LDA; $\Delta S = 6.8\%$; $\Delta P = 7.1\%$ for SVM). Note that in this case, when comparing between identifications with different number of classes (12 or 8 classes for three or two effort levels, respectively), accuracy and specificity are not the appropriate indices, as described in (Rojas-Martínez et al., 2013). These two measures are biased by the high number of observations not belonging to a given group and correctly identified as members of the other groups (TN). Thus, because of the higher number of classes, and consequently, higher number of TN observations, these indices tend to have seemingly higher results of identification of tasks and three effort levels. In this comparison, S and P are more appropriate measures because they are not affected by the number of TN (see Eq. 2.4 to Eq. 2.7) but by the number of observations for each group that were

Table 2.5: LDA identification of tasks and three effort levels

	Accuracy	**Sensitivity**	**Precision**	**Specificity**
Flexion 10% MVC	89.4% ± 1.1%	58.5% ± 5.5%	40.6% ± 4.0%	92.2% ± 1.0%
Flexion 30% MVC	89.6% ± 0.8%	22.6% ± 7.4%	32.1% ± 7.2%	95.7% ± 0.9%
Flexion 50% MVC	91.0% ± 1.0%	44.5% ± 8.2%	46.1% ± 6.2%	95.3% ± 0.9%
Flexion Average	**90.0% ± 1.0%**	**41.9% ± 7.0%**	**39.6% ± 5.8%**	**94.4% ± 1.0%**
Extension 10% MVC	88.0% ± 1.0%	32.6% ± 4.0%	30.0% ± 3.6%	93.0% ± 1.0%
Extension 30% MVC	88.9% ± 0.8%	37.9% ± 6.0%	35.0% ± 3.9%	93.6% ± 0.9%
Extension 50% MVC	89.5% ± 0.9%	40.7% ± 4.7%	38.3% ± 4.8%	94.0% ± 0.9%
Extension Average	**88.8% ± 0.9%**	**37.1% ± 4.9%**	**34.4% ± 4.1%**	**93.5% ± 1.0%**
Supination 10% MVC	89.3% ± 0.8%	46.8% ± 6.3%	38.4% ± 3.5%	93.2% ± 0.9%
Supination 30% MVC	90.0% ± 1.0%	31.1% ± 4.4%	38.0% ± 5.9%	95.3% ± 0.9%
Supination 50% MVC	92.7% ± 0.7%	56.6% ± 5.4%	56.0% ± 4.1%	95.9% ± 0.7%
Supination Average	**90.6% ± 0.8%**	**44.8% ± 5.4%**	**44.1% ± 4.5%**	**94.8% ± 0.8%**
Pronation 10% MVC	92.1% ± 0.9%	55.4% ± 4.6%	53.0% ± 5.5%	95.5% ± 1.0%
Pronation 30% MVC	89.3% ± 0.5%	15.9% ± 4.5%	26.4% ± 5.4%	96.0% ± 0.7%
Pronation 50% MVC	89.5% ± 0.8%	33.3% ± 5.7%	35.9% ± 4.7%	94.6% ± 0.8%
Pronation Average	**90.3% ± 0.7%**	**34.9% ± 5.0%**	**38.4% ± 5.2%**	**95.4% ± 0.8%**
AVG all patients	**89.9% ± 0.9%**	**39.7% ± 5.6%**	**39.1% ± 4.9%**	**94.5% ± 0.9%**
AVG C4 patients	**93.7% ± 0.8%**	**62.3% ± 7.3%**	**62.7% ± 5.8%**	**96.6% ± 0.8%**

Table 2.6: LDA identification of tasks and low and moderate effort levels

	Accuracy	**Sensitivity**	**Precision**	**Specificity**
Flexion low	87.8% ± 1.3%	60.2% ± 4.2%	51.1% ± 4.3%	91.7% ± 1.3%
Flexion moder.	92.8% ± 0.9%	62.8% ± 6.5%	76.1% ± 4.8%	97.1% ± 0.9%
Flexion Average	**90.3% ± 1.1%**	**61.5% ± 5.4%**	**63.6% ± 4.6%**	**94.4% ± 1.1%**
Extension low	85.3% ± 1.3%	39.0% ± 5.3%	41.0% ± 4.8%	91.9% ± 1.3%
Extension moder.	86.0% ± 1.3%	55.9% ± 5.9%	45.2% ± 3.8%	90.2% ± 1.5%
Extension Average	**85.6% ± 1.3%**	**47.5% ± 5.6%**	**43.1% ± 4.3%**	**91.1% ± 1.4%**
Supination low	87.4% ± 1.1%	58.2% ± 4.2%	49.9% ± 3.6%	91.6% ± 1.2%
Supination moder.	93.0% ± 1.0%	68.9% ± 5.2%	74.1% ± 5.7%	96.5% ± 1.1%
Supination Average	**90.2% ± 1.0%**	**63.5% ± 4.7%**	**62.0% ± 4.7%**	**94.0% ± 1.2%**
Pronation low	88.8% ± 1.0%	55.6% ± 6.0%	55.5% ± 4.5%	93.6% ± 1.3%
Pronation moder.	86.9% ± 0.8%	31.7% ± 4.6%	47.0% ± 4.5%	94.8% ± 1.0%
Pronation Average	**87.9% ± 0.9%**	**43.6% ± 5.3%**	**51.3% ± 4.5%**	**94.2% ± 1.2%**
AVG all patients	**88.5% ± 1.1%**	**54.0% ± 5.2%**	**55.0% ± 4.5%**	**93.4% ± 1.2%**
AVG C4 patients	**94.3% ± 1.0%**	**77.1% ± 6.4%**	**78.4% ± 5.1%**	**96.7% ± 1.0%**

Table 2.7: SVM identification of tasks and three effort levels

	Accuracy	Sensitivity	Precision	Specificity
Flexion	98.1% ± 0.4%	88.6% ± 3.7%	89.5% ± 3.2%	99.0% ± 0.3%
Extension	97.6% ± 0.4%	85.4% ± 3.7%	85.4% ± 3.3%	98.7% ± 0.4%
Supination	97.8% ± 0.4%	87.5% ± 3.3%	86.4% ± 3.9%	98.7% ± 0.4%
Pronation	96.6% ± 0.4%	79.3% ± 5.0%	79.9% ± 3.8%	98.2% ± 0.5%
AVG all patients	**97.5% ± 0.4%**	**85.2% ± 3.9%**	**85.3% ± 3.5%**	**98.7% ± 0.4%**
AVG C4 patients	**97.3% ± 0.5%**	**84.1% ± 5.4%**	**84.4% ± 4.5%**	**98.6% ± 0.5%**

Table 2.8: SVM identification of tasks and low and moderate effort levels

	Accuracy	Sensitivity	Precision	Specificity
Flexion	98.7% ± 0.4%	94.4% ± 2.7%	95.6% ± 2.2%	99.4% ± 0.3%
Extension	97.9% ± 0.4%	91.5% ± 3.7%	92.4% ± 3.0%	98.8% ± 0.5%
Supination	97.9% ± 0.6%	92.8% ± 2.8%	91.2% ± 3.2%	98.7% ± 0.5%
Pronation	97.5% ± 0.6%	89.5% ± 3.5%	90.6% ± 3.1%	98.6% ± 0.5%
AVG all patients	**98.0% ± 0.5%**	**92.0% ± 3.2%**	**92.4% ± 2.9%**	**98.9% ± 0.5%**
AVG C4 patients	**97.8% ± 0.7%**	**91.4% ± 3.9%**	**91.7% ± 3.6%**	**98.8% ± 0.6%**

correctly classified to that group (TP) with respect to the number of those that were wrongly classified to another group (FN), and with respect to those that were incorrectly classified as members of the group (FP), respectively. Finally, in all cases, the SVM-based identification outperformed the LDA-based both in the conjoint identification of tasks and three effort levels ($\Delta Acc = 7.6\%$; $\Delta S = 45.5\%$; $\Delta P = 46.1\%$; $\Delta SP = 4.1\%$) and in the identification of tasks and low and moderate effort levels ($\Delta Acc = 9.5\%$; $\Delta S = 38.0\%$; $\Delta P = 37.4\%$; $\Delta SP = 5.4\%$). The interactions between classifiers, tasks, and effort levels were analyzed using a repeated measures analysis of variance. The post hoc pairwise comparison of means was performed with application of the Bonferroni correction factor. Effects were considered to be significant at p-value $p = 0.01$. The interaction between the classifier and the task, as well as the interaction between the classifier and the effort level were both found significant. However, the post hoc pairwise comparison of means showed no significant differences between the identification results across individual tasks for the SVM classifier, whereas the extension and, especially, the pronation had much lower identification indices than the flexion and the supination for the LDA classifier. When considering the influence of the classifier on the identification of effort level, the detection of 10% MVC had in average the highest performance in both classifiers, but the LDA

Table 2.9: Identification of tasks using a subset of electrodes: Classification indices using a 3x3 electrode grid located randomly in each muscle. Results are averaged within the group of all patients (top) and group of patients with C4 level of injury (bottom).

	LDA			
	Accuracy	**Sensitivity**	**Precision**	**Specificity**
AVG all patients	79.2% ± 2.7%	58.5% ± 6.5%	58.9% ± 5.8%	86.1% ± 2.8%
AVG C4	83.5% ± 3.2%	67.1% ± 7.1%	67.5% ± 7.1%	80.0% ± 3.1%

	SVM			
	Accuracy	**Sensitivity**	**Precision**	**Specificity**
AVG all patients	94.8% ± 1.1%	89.7% ± 3.3%	89.7% ± 2.8%	96.5% ± 1.0%
AVG C4	94.8% ± 1.4%	89.6% ± 3.8%	89.8% ± 3.9%	96.5% ± 1.5%

detected 30% MVC effort level much worse than the 50% MVC effort level, whereas there was no significant difference in detection between 30% MVC and 50% MVC using the SVM.

2.3.4 Classification Using Smaller Arrays of Electrodes

Subsets of electrodes (3×3 electrodes) were considered in the identification of tasks and levels of effort to evaluate the classification performance using a lower number of electrodes at different positions. Four different locations within the area covered by the entire array were selected randomly for each muscle to evaluate the impact of their placement on the identification performance. The identification was carried out following the same procedure as considering the entire array but using only the intensity features, because the spatial information could not be measured using these small arrays. The average results of the identification of tasks can be seen in Table 2.9, whereas the average results of the identification of tasks and three effort levels can be seen in Table **??**.

Results obtained using 3×3 electrode grids were slightly worse than the results obtained using the entire electrode arrays (see Tables 2.3 and 2.4). In addition, the classification indices of conjoint identification of tasks and effort levels were very low, inferring that the results obtained by adding spatial features (see Tables 2.5 and 2.7) cannot be reached with a smaller grid of electrodes.

Table 2.10: Identification of tasks and three effort levels using a subset of electrodes: Classification indices using a 3x3 electrode grid located randomly in each muscle. Results are averaged within the group of all patients (top) and group of patients with C4 level of injury (bottom).

	LDA			
	Accuracy	**Sensitivity**	**Precision**	**Specificity**
AVG all patients	88.1% ± 1.3%	28.7% ± 7.4%	28.3% ± 6.4%	93.5% ± 1.5%
AVG C4	89.7% ± 1.6%	38.4% ± 9.1%	38.8% ± 9.1%	94.4% ± 1.6%

	SVM			
	Accuracy	**Sensitivity**	**Precision**	**Specificity**
AVG all patients	93.8% ± 8.5%	62.9% ± 7.5%	63.3% ± 5.7%	96.6% ± 0.8%
AVG C4	93.8% ± 1.0%	62.9% ± 8.6%	63.6% ± 6.9%	96.6% ± 1.0%

2.4 Discussion

In order to demonstrate the existence of distinguishable group-specific patterns in HD-EMG, the identification of different tasks was performed. Within-group identification of motion intention at different effort levels was tested on nine patients with iSCI performing four upper limb tasks (flexion/extension of the elbow and supination/pronation of the forearm) at three different effort levels (10%, 30%, and 50% MVC).

Although a single type of a classifier would be sufficient to demonstrate the existence of different patterns, for an additional verification two types of classifiers were evaluated in the identification of motion intention: LDA and SVM. The former is a classical, simple, and computationally efficient classification method, whereas the latter is a more powerful classifier that can employ a nonlinear transform of features to improve their separability among classes. In this paper, a SVM with radial kernel was considered. Although the SVM is superior in classification performance, the LDA is commonly used in myocontrol applications because of its simplicity and performance in real-time. However, with the increasing computational power of new computer generations, SVM could become more common in these applications.

The identification of tasks was tested using two feature sets: 1) the average intensities of HD-EMG activation maps (I) of five muscles and 2) the combination of average intensities and centers of gravity (I+CG) of the activation maps of five muscles. On the other hand, a conjoint identification of tasks and effort levels was designed as two-step classifier, following the procedure described by Rojas et al. (Rojas-Martínez et al., 2013) and tested on a healthy population. The first step comprised the identification of tasks using a combination of intensity and spatial features of all five muscles, whereas in the second step the levels of effort were identified separately for each task. The effort levels were identified using a combination of the intensity and spatial features of agonist-antagonist muscle pairs involved in the task (Rojas-Martínez et al., 2013).

HD-EMG activation maps were calculated for all exercises and compared among patients.

Rojas-Martínez et al. (**?**) calculated the relative standard deviation between maps within a group of healthy subjects (17.4% in average), reporting an increase in standard deviation between maps with increasing effort levels (12.1%, 16.6%, and 23.6% for 10%, 30%, and 50% MVC, respectively). As expected, the dispersion between maps of iSCI patients was considerably higher (56% in average), but the variability was similar in the case of patients with iSCI (Table 1). However, when maps were compared among patients with the same level of injury, the standard deviation between maps was greatly reduced (19% in average). Moreover, the variability was higher for muscles of the upper-arm (biceps and triceps) than for forearm muscles. This reduction could be either due to a distinct activation, specific to the level of injury, or because during the rehabilitation process patients developed similar activation patterns. This is an important finding that has to be taken into account when training a classifier for a group of patients. Muscle activation patterns in patients differed from those of healthy subjects in (Rojas-Martínez et al., 2012): the Biceps Brachii was more active during supination than during flexion; the Pronator Teres was more active during supination and especially during flexion than during pronation. This could be because both muscles are particularly affected by the iSCI at the level of C4 (Young).

Furthermore, the results using the LDA showed much better identifications within the group of patients with a C4 level of injury than within the group of all patients. These findings could be related to a higher homogeneity among patients with the same level of injury. The combination of intensity and center of gravity performed better than only intensity features. These results showed that similar patterns exist in spite of the diverse nature of their injuries. This correlation exists not only in the average intensity of the HD-EMG activation maps, but also in the spatial distribution of EMG intensity, which justifies the choice of these intensity and spatial features for automatic identification.

Finally, a considerable improvement was observed when using the SVM instead of the LDA, reaching the following results: 1) excellent automatic task identification even in the group of all patients (Acc = 99.0%, S = 97.9%, P = 98.0%, and SP = 99.3%), 2) a good combined classification of four tasks and three effort levels also in the group of all patients (Acc = 97.5%, S = 85.2%, P = 85.3%, and SP = 98.7%) which is even better in 3) conjoint identification of four tasks and low or moderate effort levels (Acc = 98.0%, S = 92.0%, P = 92.4%, and SP = 98.9%). In spite of the previous reports suggesting the greater importance of selection of the features than the selection of the classifier, our results have shown that both have considerable impact on the identification.

Several array subsets corresponding to 3×3 square grids of channels (IED = 10 mm) located at different positions were also used to evaluate the possibility of task identification using a much smaller number of electrodes. In this case, the results were considerably worse, especially when using the LDA classifier. Due to the small region covered by electrodes in each muscle, the spatial information could not be extracted and it was not possible to increase the performance as in the case of using all the electrodes.

Although this study presents an important improvement in the identification of motion intention, it is important to mention that the recordings were carried out during highly controlled isometric contractions. Therefore, even though the findings are promising, they are only a step towards final real-time applications involving free movements and multiple DoFs.

The results show that the use of a SVM-based classifier is indeed a promising approach in myocontrol-oriented pattern recognition applications. Moreover, even though a different activation pattern can be expected in subjects with neurological impairment, as in the present case, such pattern can still be associated with task and level-dependent changes in the spatial distribution of the intensity, as has been previously observed in non-injured subjects (Rojas-Martínez et al., 2012).

2.5 Conclusions

Group-specific identification of motion intention in impaired patients has a potential to improve the translation of pattern recognition techniques to clinical practice. Unfortunately, group-specific design is a difficult topic because it assumes strong task-related and level of effort-related co-activation patterns among patients, but given the diverse nature of injuries and the high inter-patient variability, co-activation patterns are weak.

This study shows that muscular co-activation patterns in intensity and spatial distribution indeed exist. Furthermore, it shows that stronger co-activation patterns can be found between patients of the same level of injury. Whether because of the rehabilitation process or the level of injury, muscle control strategies are similar for the group of patients with an injury at C4, which makes them a more homogenous population and enables the control of universal assistive devices with higher reliability. In summary, in spite of the difficulty to identify both task and effort level in patients with iSCI, very promising results were found to provide a useful estimation of motion intention.

2.6 Acknowledgements

Special acknowledgement to Ursula Costa and Josep Medina as assistant and Head of the Functional Rehabilitation service respectively, of the Neurorehabilitation Hospital Institut Guttmann for their collaboration in patients recruitment and clinical support during the experiments carried out at the same Hospital.

This work has been partially supported by the Spanish Ministry of Economy and Competitiveness-Spain (project DPI2014-59049-R), and by the FI grant from the AGAUR, Generalitat de Catalunya, Spain.

Chapter 3

A Novel Spatial Feature for the Identification of Motor Tasks Using High-Density Electromyography

Published as: Jordanić, M., Roja-Martínez, Mañanas, M.A., Alonso J.F., Marateb H.R. A Novel Spatial Feature for the Identification of Motor Tasks Using High-Density Electromyography *Sensors* 17(7):1597, 2017

doi: 10.3390/s17071597

Impact Factor: 2.077; Position: 10 of 58 (Q1) INSTRUMENTS AND INSTRUMENTATION.

Abstract: Estimation of neuromuscular intention using electromyography (EMG) and pattern recognition is still an open problem. One of the reasons is that the pattern-recognition approach is greatly influenced by temporal changes in electromyograms caused by the variations in the conductivity of the skin and/or electrodes, or physiological changes such as muscle fatigue. This paper proposes novel features for task identification extracted from the high-density electromyographic signal (HD-EMG) by applying the mean shift channel selection algorithm evaluated using a simple and fast classifier-linear discriminant analysis. HD-EMG was recorded from eight subjects during four upper-limb isometric motor tasks (flexion/extension, supination/pronation of the forearm) at three different levels of effort. Task and effort level identification showed very high classification rates in all cases. This new feature performed remarkably well particularly in the identification at very low effort levels. This could be a step towards the natural control in everyday applications where a subject could use low levels of effort to achieve motor tasks. Furthermore, it ensures reliable identification even in the presence of myoelectric fatigue and showed robustness to temporal changes in EMG, which could make it suitable in long-term applications.

Keywords: high-density electromyography; pattern recognition; myoelectric control; mean shift; prosthetics

3.1 Introduction

Electromyography (EMG) is a technique for recording the electrical activity produced by skeletal muscles. The EMG signal is a summation of action potentials produced by muscle fibers, directly triggered by the action potentials traveling along motor neurons (Farina et al., 2010). Since EMG is an important source of neural information, it has been extensively studied in the field of human-machine interfacing (Nazmi et al., 2016; Hakonen et al., 2015). Applications of EMG include the control of neurorehabilitation devices such as prostheses (**?**Li et al., 2010), rehabilitation robots (Marchal-Crespo and Reinkensmeyer, 2009; **?**), and identification of muscle anatomical structure (Marateb et al., 2016), but also implementations in leisure activities such as sports (Verikas et al., 2016) and computer games (van Dijk et al., 2016).

EMG signals could be recorded either non-invasively (surface EMG, sEMG) or invasively with needle and wire electrodes (intramuscular EMG, iEMG) (Marateb et al., 1999). Although the iEMG has higher signal-to-noise ratio, both approaches provide a similar quality of identification of upper-arm motor task (Hargrove et al., 2007). Moreover, sEMG is preferred as it is recorded non-invasively.

The pattern recognition approach has been recently used in research laboratories as a state-of-the-art method to decode neural information. Its main advantage over conventional systems is the instant activation of a task belonging to any of the available degrees-of-freedom (DoFs). Many classifiers such as linear discriminant analysis (LDA), support vector machine, and artificial neural network were successfully employed for this purpose with a high identification fidelity (Oskoei and Hu, 2007), but many authors agree that the choice of the features is more important than the choice of the classifier (Hargrove et al., 2007). Hence, simple and fast classifiers are preferred, among which the LDA is commonly used and has become a general recommendation (Hakonen et al., 2015; Huang et al., 2009). In addition, different studies have focused on pattern recognition from the analysis of isometric contractions for myoelectric control, especially when considering subjects with neuromuscular impairment (in stroke for example) (Celadon et al., 2016) and even for prostheses control for amputees (Ameri et al., 2012). Additional examples can be found in (Li et al., 2013; Jordanic et al., 2016; Jordanić et al., 2016).

Features can be calculated in time, frequency/scale, and time-frequency/scale domain (Nazmi et al., 2016; Hakonen et al., 2015; Oskoei and Hu, 2007). Time domain features are usually used because of their computational simplicity and good performance (Hakonen et al., 2015). Additionally, they can be combined with other features to increase the performance, e.g., autoregressive features (Hargrove et al., 2007).

The influence of the physiological (e.g., muscle fatigue) or non-physiological (electrode-skin impedance) non-stationarity of the EMG features is a big issue in neuromuscular control. As a solution, Vidovic et al. (Vidovic et al., 2016) and Hahne et al. (Hahne et al., 2015) proposed a real-time retraining of the classifier where the parameters are constantly updated. Liu et al. (Liu et al., 2016) proposed a universal LDA classifier which was trained during different days and then combined. Such methods adapt the model to changes in the features, rather than using robust features.

Moreover, the variation of force can affect the identification (Tkach et al., 2010). Scheme and Englehart (Scheme and Englehart, 2013) recommended to train the classifier using all effort levels, whereas He et al. (He et al., 2015) tackled the problem using a feature set based on the frequency content of the signal and muscle coordination.

With the recent introduction of high-density EMG (HD-EMG) (Merletti et al., 2009), i.e., multichannel EMG recorded using 2D grids of closely spaced sEMG electrodes, multiple studies have reported improvement in task identification. Stango et al. reported that spatial features extracted from the HD-EMG are robust to the electrodes shift. Geng et al. (Geng et al., 2016) and Du et al. (Du et al., 2017) exploited the power of deep convolutional network to design gesture recognition classifier that classifies instantaneous maps, i.e., raw HD-EMG samples. Hahne et al. extracted features using spatial filters optimized to increase separability between different classes (Hahne et al., 2012). This methods exploit the information about spatial muscle activation pattern extracted from the HD-EMG and the fact that the myoelectric activity over different parts of muscle depends on the various factors (e.g., contraction level (Holtermann et al., 2005), duration of the contraction (Tucker et al., 2009), and joint position (Vieira et al., 2010)) and can be useful in differentiation between tasks.

In our previous work, we used the center of gravity as a feature to describe spatial patterns in HD-EMG (Jordanic et al., 2016; Jordanić et al., 2016; Rojas-Martínez et al., 2013). In this work, we propose a new spatial feature for task identification based on the modified mean shift algorithm. Novel features were evaluated in the identification of four isometric motor tasks of the upper-limb (flexion/extension, supination/pronation of the forearm) using the LDA classifier. The proposed features were tested in three conditions: when training set and test set were recorded at the same time (time-dependent changes in the signal are minor), when test set was recorded after training set, and during the fatiguing exercise. In addition, features were tested during the identification of task recorded at different effort levels. The proposed features proved to improve the identification and are especially useful in extreme cases like identification of tasks recorded at very low effort level or identification of tasks during fatigue. These results confirm the usefulness of information of spatial distribution of myoelectric intensity over the muscle in discrimination between tasks. The rest of the paper is organized as follows: in the next section, information about the experimental protocol and the task identification method used in this study is presented. Section 3 provides the results of the identification using the proposed features and its comparison with the previously established features. The discussion is provided in Section 4 and finally, the conclusions are summarized in Section 5.

3.2 Materials and Methods

3.2.1 Instrumentation and Measurement Protocol

Eight healthy subjects (age: 36 ± 5 years; height: 177 ± 5 cm; weight: 75 ± 9 kg; body mass index: 23.7 ± 2.3) participated in the experiment. They reported no pain, and previously had not suffered any injuries or neuromuscular upper limb impairments. The study was conducted in accordance with the Declaration of Helsinki and subsequent amendments concerning research in humans and was approved by the University Ethics Committee and the local government. Recordings and results were documented with the registration number, which corresponded to the Spanish ministry project MICINN (TEC2008-02274): “Analysis of the dynamic interactions in non-invasive multichannel biosignals for rehabilitation and therapy”. All subjects gave their written informed consent to participate in the experimental protocol.

Subjects performed four different isometric upper-limb tasks with two degrees of freedom: flexion/extension and supination/pronation of the forearm. During the experiment they were seated upright with their back being straight. Their dominant arm was positioned in the sagittal plane with the elbow flexed at 45 degrees and the forearm positioned in the middle between supination and pronation, thumb pointing upwards (Figure 3.1). To avoid muscle activation due to gripping, their hands were fixed at the wrist using a mechanical brace. The brace also contained two torque meters that measured exerted torque at the elbow joint.

HD-EMG was measured on five superficial muscles involved in the presented tasks: biceps brachii, triceps brachii, brachioradialis, anconeus, and pronator teres. Signals were recorded using three two-dimensional electrode arrays manufactured as silver-plated eyelets (2.5 mm radius) positioned in a quadrature grid with a 10 mm inter-electrode distance and embedded in a non-conductive fabric (Figure 3.1a).

After the skin was shaved, cleaned, and treated with abrasive gel, the following electrode arrays were positioned over the upper limb using elastic straps: two electrode arrays (dimensions: 8 rows × 15 columns) were positioned on the upper arm covering biceps brachii and triceps brachii muscles. The center of each electrode array was placed according to the positions recommended by the SENIAM project (Hermens and Freriks, 1999). The third electrode array was placed over

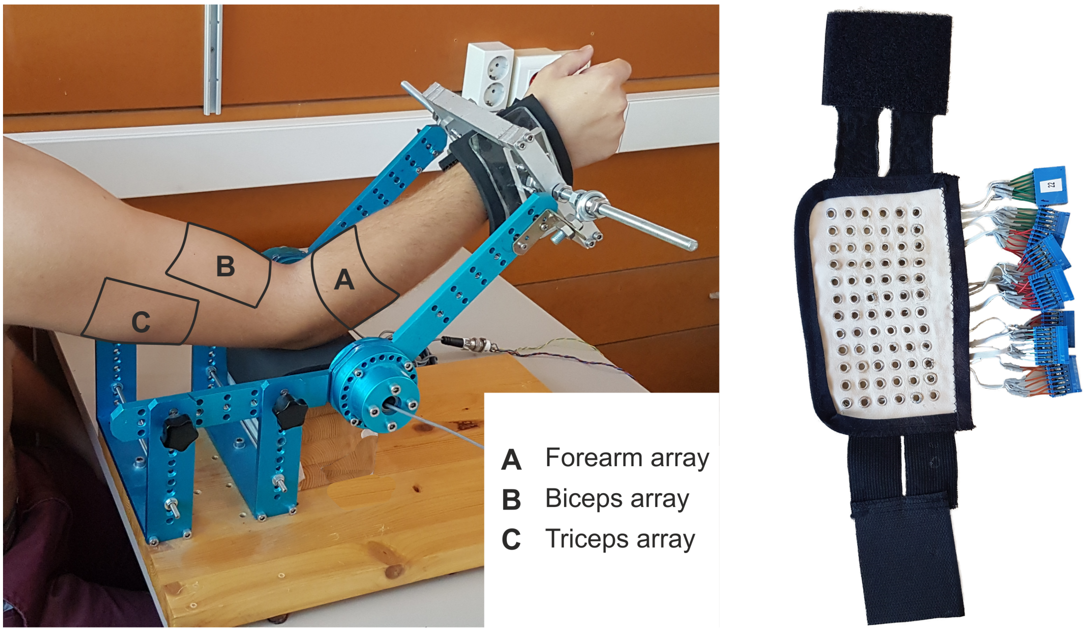

(a) (b)

Figure 3.1: Figure shows (a) the position of the arm in the mechanical brace during the recording with the marked outlines of the electrode arrays; and (b) an electrode array.

the forearm, with the first row of electrodes approximately 2 cm below elbow crest, covering brachioradialis, anconeus, and pronator teres muscles. A line connecting the origin and insertion of the targeted muscles were previously marked on the skin and the electrode array was placed to optimally cover these muscles. The forearm electrode array had six rows and between 17 and 19 columns, depending on the forearm circumference. After positioning the electrodes, the conductive gel was applied through the eyelet of each electrode (20 μL) using the dosimeter (Multipette Plus, Eppendorf, Germany).

HD-EMG signals were recorded in monopolar mode using three commercially available amplifiers with simultaneous sampling (EMG-USB, 128 channels, 2048 Hz sampling frequency, 10–750 Hz passband, manufacturer LISiN-OT Bioelettronica, Turin, Italy). Torque exerted on the elbow joint was measured using two torque transducers (OT Bioelettronica, range 150 Nm) and was displayed to the patient in real time. The detailed information on the instrumentation settings can be found in (Rojas-Martínez et al., 2012).

Prior to the experiment, the maximal voluntary contraction (MVC) was measured for each task as the maximal of three consecutive trials. In the first part of the experiment subjects were instructed to perform four defined tasks at three randomized different effort levels: 10%

MVC, 30% MVC, and 50% MVC. Having been instructed to maintain the target level for 10 s, the exerted torque was displayed to the subjects. Tasks were performed in random order and between two consecutive recordings there was a two-minute rest to prevent cumulative fatigue.

Approximately 30 min (33 ± 3 min) after the first part of the protocol, endurance measurements were performed. Subjects were instructed to perform each task at 50% MVC until failure. After each measurement, subjects rested for five min.

3.2.2 HD-EMG Processing

The recorded HD-EMG signals were band-pass filtered using a 4^{th} order Butterworth filter, with the cut-off frequencies of 15 Hz and 350 Hz, in the forward and reverse direction as to minimize the distortions. Outlier channels were automatically identified using a previously described algorithm (Rojas-Martínez et al., 2012). HD-EMG recordings were divided into non-overlapping 150 ms time windows and the average HD-EMG activation maps were then calculated for each window in all three electrode arrays (biceps, triceps, forearm) using the RMS values. Activation maps can be conceptually perceived as images where pixels correspond to channels, and pixel intensities correspond to the muscle activation map in each channel. They were calculated as:

$$AM_{i,j} = \sqrt{\frac{1}{N}\sum_{n=0}^{N-1} EMG_{i,j}^{2}[n]} \tag{3.1}$$

where AM is the activation map, N corresponds to the number of samples in each window (given a sampling frequency of 2048 Hz, $N = 410$), and $EMG_{i,j}$ denotes the EMG signal recorded by the electrode located at (i, j) position in the recording array. Pixels in AM corresponding to the outlier channels previously identified as artifacts were discarded and substituted using the triangular interpolation (Rojas-Martínez et al., 2012). Examples of torque and EMG signals can be found in the Appendix B.

3.2.3 Feature Extraction

Identification was performed using the combination of intensity features and spatial features (Figure 3.2). Spatial features were extracted using the mean shift algorithm (Comaniciu and Meer, 2002), a non-parametric approach to estimate modes (local maxima) of the underlying density function by an iterative procedure. The details of the mean shift algorithm are provided in the Appendix A and are briefly discussed here. A centroid point y was positioned at a random point in the space and the mean value was calculated for all points x, which were located within the Euclidean distance, i.e., bandwidth h, from the current centroid. This mean value was assigned as a new position of a centroid y in the next iteration. The procedure can be mathematically defined as:

$$y_{i+1} := \left. \frac{\sum_{j=1}^{M} x_j}{M} \right|_{\forall x \, s.t. \, \|x - y_i\| \leq h} \tag{3.2}$$

where x_j $(j = 1, 2, \ldots, M)$ are samples of the unknown distribution, y_i is the centroid in the i^{th} iteration of the algorithm and the h is a bandwidth parameter. The algorithm stops when the position of the centroid (y) remains constant in consecutive iterations (up to a tolerance). This centroid y is considered to be a mode of the underlying density function. In this study, modes of the density function of RMS activation maps were found using the mean shift algorithm implemented in Python (Pedregosa et al., 2011) and were used as features in the identification.

The bandwidth h was estimated automatically for each map. The maximum Euclidean distance between k nearest neighbors (where k was set to 50% of the total number of elements in the map) was calculated for every sample and the average of the maximum distances was calculated. The bandwidth used in this paper was obtained by multiplying this average distance by a bandwidth factor of 0.5, selected as a tradeoff between the amount of information and the processing time.

Prior to using the mean shift algorithm, each RMS activation map was transformed to a matrix of n rows, each row a channel, by three columns where the first two corresponded to the x, and y location of the channel in the activation map and the third to its intensity as estimated from the RMS of the signal. Since we used the spherical kernel, i.e., the bandwidth h had an equal value in all three dimensions, data was standardized to have zero mean and unity variance in

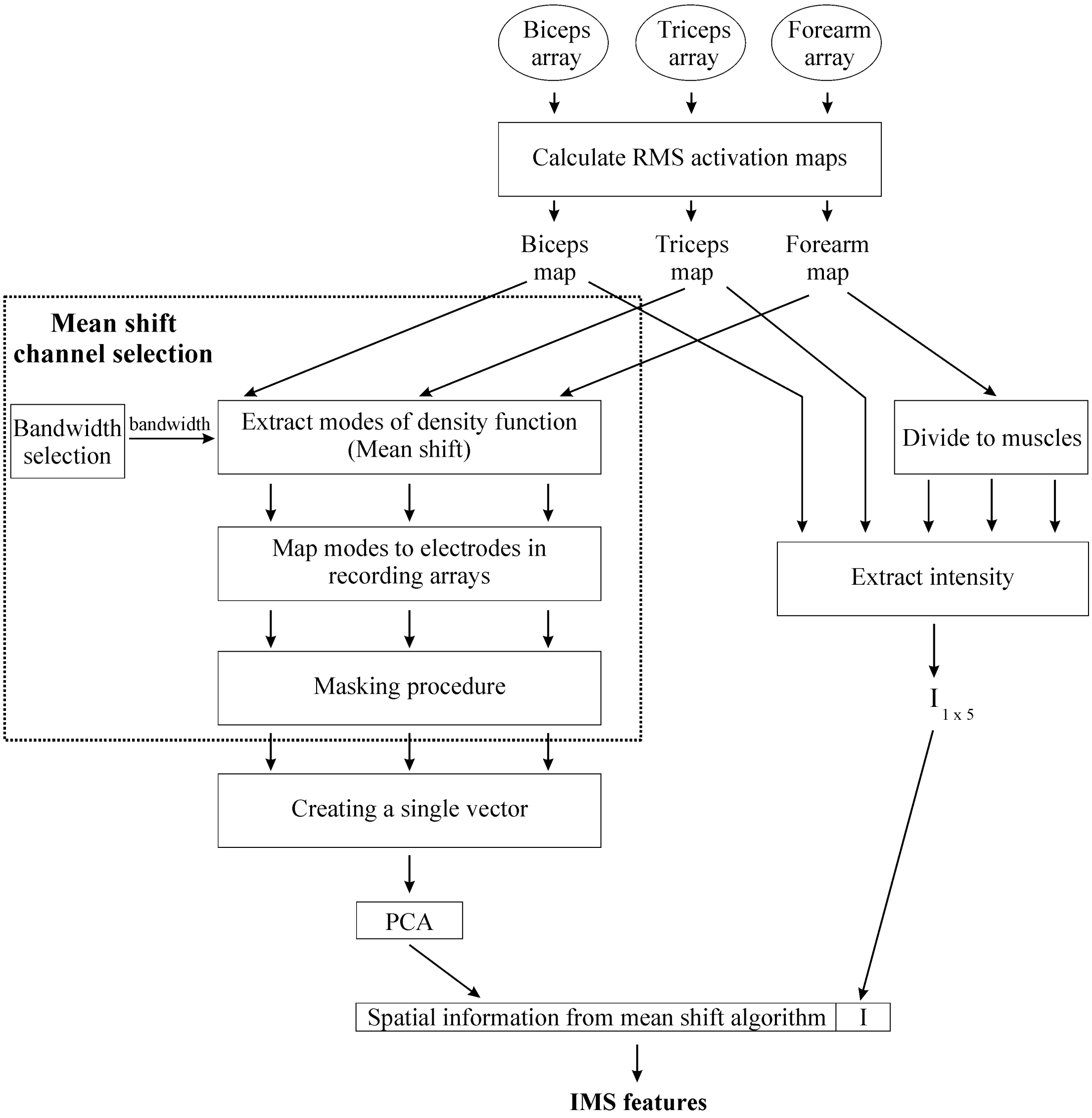

Figure 3.2: Feature extraction flowchart.

all three dimensions.

A matrix of zeros with the same dimension of the electrode array was then created. Each mode detected by the mean shift algorithm was mapped to the closest location of the electrode in the array and its value was set to one. The result of this step was a binary image where the number of nonzero elements was equal to the number of detected modes. The procedure was repeated for all three activation maps. The resulting matrices were reshaped as a single $1-d$ vector in which the number of elements equaled to the total number of recorded EMG channels (for all three electrode arrays).

Principal component analysis (PCA) was then used for reducing the dimensionality of the feature space. A cumulative percentage of variance of 90% was used for dimensionality reduction, i.e., after the transformation to the orthonormal space, features were ordered by variance, and only the features explaining at least 90% of the cumulative variance were kept (Valle et al., 1999). This reduced spatial feature set was then combined with the intensity features.

For calculation of intensity features, HD-EMG activation maps were segmented into areas covering the targeted muscle following the same procedure described in (Rojas-Martínez et al., 2012) and repeated in (Rojas-Martínez et al., 2013). Segmentation discards the map areas not covering the recorded muscle (e.g., edges of maps), and also divides the forearm map into three different maps which correspond to forearm muscles. From the resulting five segmented activation maps (biceps brachii, triceps brachii, brachioradialis, anconeus, and pronator teres), intensity features (I) were calculated as:

$$I = \log_{10} \frac{1}{N} \sum_{i,j} SAM_{i,j} \tag{3.3}$$

where I is the intensity feature, $SAM_{i,j}$ is the intensity value of the pixel at location (i, j) in the segmented activation map SAM, and N is the total number of pixels in that map. Therefore, this procedure extracts five intensity features, one for each muscle. By concatenation, these intensity features were combined with the reduced spatial features into a single feature vector. These generated features were used in the identification and will be referred to as IMS from now on. Results were compared with the previously proposed feature set: a combination of intensity and center of gravity (ICG) of segmented activation maps (Jordanic et al., 2016; Jordanić et al., 2016; Rojas-Martínez et al., 2013). In this feature set, the center of gravity represents the traditional approach of describing the spatial information of intensity distribution over the muscle. The center of gravity (CG) has two dimensions and was calculated for each of the five muscles as:

$$CG = \frac{\sum_{i,j} SAM_{i,j} \begin{bmatrix} i \\ j \end{bmatrix}}{\sum_{i,j} SAM_{i,j}} \tag{3.4}$$

Therefore, ICG is a feature vector of 15 dimensions. Identification was also performed using only intensity features (I), and two classical features, single differential signal (Diff) and time-domain features (TD). One differential signal was obtained from each of five muscles using a pair of electrodes selected within the electrode arrays. Two adjacent electrodes located over the location proposed by the SENIAM were used to obtain the differential signal. Feature used in the analysis is RMS value of the differential signal calculated over the 150 ms time window. On the other hand, five TD features were calculated for each recorded channel. These features were firstly proposed by Hudgins (Parker et al., 2006) and used many times in literature (for example [39]). They were: RMS value, mean absolute value, number of zero crossings, waveform length, and number of slope sign changes. To be reduced in number, obtained features were projected to the space of lower dimensionality using PCA. As for the calculation of MS, only projections explaining 90% of variance were kept.

3.2.4 Task Identification

LDA was used for the identification of motor tasks. Task identification was evaluated using the repeated holdout method ($N = 20$). Observations were randomly assigned to the training set and the test set (70% to the training set) using stratified sampling. Both the PCA transformation function and the LDA discriminant function were calculated on the training set, and evaluated on the test set. Only the results of the test set are presented. Identification results were expressed in terms of sensitivity (S) and precision (P), defined as:

$$S = \frac{TP}{TP + FN} \tag{3.5}$$

$$P = \frac{TP}{TP + FP} \tag{3.6}$$

where TP (true positive) is the number of samples that were correctly classified, FN (false negative) is the number of samples belonging to a certain class and erroneously classified into another class, whereas FP (false positive) is the number of samples incorrectly classified to a certain class (**?**).

The identification was evaluated under various conditions:

- Short-term identification
- Long term identification
- Identification during fatigue

In short term identification, the training and validation sets were recorded at the same time. This are in fact the "perfect conditions" where the slow time-dependent changes in the sEMG signal associated with the recordings were minor. The dataset was composed of the recordings obtained in the first part of the measurement protocol. Two types of identification were tested: identification of task and identification of task and effort level. In the identification of task, only the task was identified, regardless of the effort level, i.e., recordings of different effort levels were pooled together to form a single class. In this experiment, there were only four classes: flexion, extension, supination, and pronation. Identification of task and effort level was designed as a two-step classifier. In the first step the task was identified, regardless of the effort level, as discussed above. In the second step, classification of three levels of effort was performed for each identified task individually. The second step consisted of four different classifiers, one classifier for the identification of the effort level of each task. For identification of effort level of a sample, the second step classifier was selected depending on the classified task in the first step (Jordanić et al., 2016). Classifiers in the second step were designed using the reduced feature set, as proposed in (Jordanić et al., 2016), where features were extracted from agonist-antagonist muscle pairs involved in the selected task, i.e., biceps brachii and triceps brachii for identification of the effort level during flexion and extension; biceps brachii, brachioradialis and anconeus for supination; and pronator teres and anconeus for pronation. Since the modes of the density function were calculated for the entire forearm array (not for each muscle separately), modes extracted from the entire forearm array were used in the identification of the effort level during supination and pronation. In the long-term identification, robustness to time effect was tested. In this part of the protocol, the training set was composed of all observations recorded in the first part of the measurement protocol, whereas the test set was composed of the first two seconds of the recordings in the second part of the protocol. Having in mind that there was a time gap between the first part of the protocol and the second part of the protocol ($\approx$30 min), using this procedure the influence of different time effects can be evaluated (e.g., drying of conductive gel). On the other hand, to prevent the effect of fatigue, only the first two seconds of the total duration of the exercise were used in the test set. Robustness of the identification was also tested during endurance tasks recorded during the second part of the recording protocol. Recordings were divided into five equal time epochs. The classifier was trained using the samples extracted from the first 20% of the total duration of recording (TDR), and was evaluated on five equally long segments throughout the exercise: 0–20% TDR, 20–40% TDR, 40–60% TDR, 60–80% TDR, and 80–100% TDR.

3.2.5 Statistical Methods

Statistical difference in performance was checked between IMS and other feature sets. The Kolmogorov-Smirnov test showed that the data significantly deviate from a normal distribution, so the non-parametric statistical Wilcoxon signed rank test was used to test for differences between distributions. In addition, the non-parametric repeated measures Friedman test was used to test the differences in identification of the task when the training set was composed of pool of all effort levels, and test set of only 10% MVC, 30% MVC, or 50% MVC. This was repeated for all feature sets. The significance level was set to $p = 0.05$. Statistical tests were performed using the IBM SPSS Statistics software package (IBM SPSS Statistics for Windows, version 20.0, released 2011; IBM Corp.: Armonk, NY, USA).

3.3 Results

3.3.1 Bandwidth and Time Window Selection

Two aspects where considered in the choice of the bandwidth factor: the average execution time of the mean shift algorithm and the amount of information, i.e., number of detected modes (Figure 3.3). The average processing time was measured on a standard desktop computer featuring an Intel® E8400 Core^{TM} 2 Duo CPU (Intel, Santa Clara, CA, USA). Both graphs show that the elbow point was at the bandwidth factor of 0.5. If the bandwidth factor is set to a lower value, both the execution time and the number of modes increase notably. A rapid increase of the number of modes for lower bandwidths implies that the mean shift algorithm is focused on local maxima, whereas the increase of the execution time increases the latency of the system. On the other hand, there was not much difference when the bandwidth factor ranges between 0.5 and 1.0, both in the number of estimated modes, and the execution time. Therefore, the range from 0.5 to 1.0 was considered of interest for the selection of the bandwidth factor.

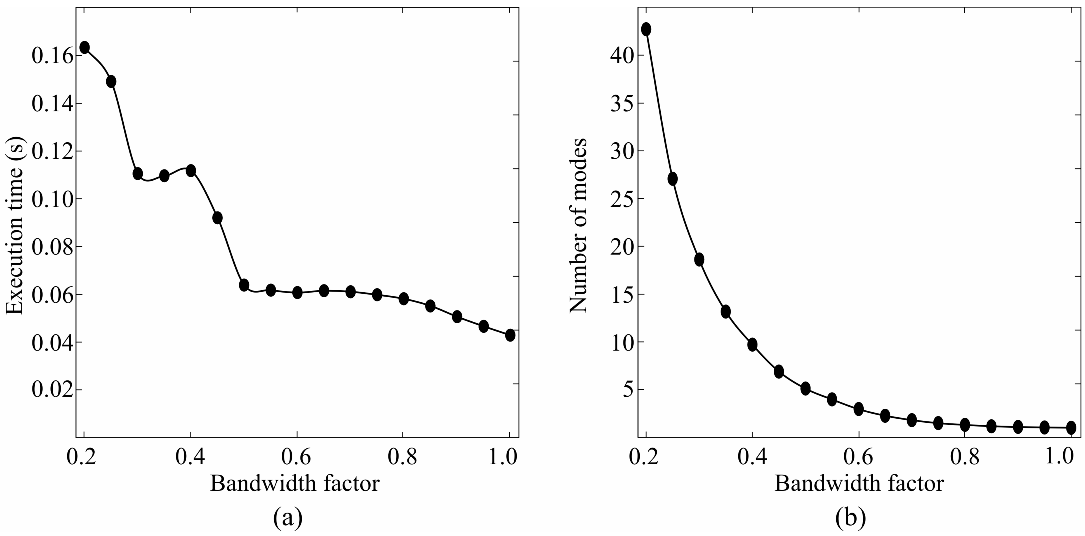

Figure 3.3: Figure shows average processing time (a) and number of estimated modes (b) of mean shift algorithm given the specific bandwidth factor in the range from 0.2 to 1.

The identification of task and the identification of task and effort level (Figure 3.4) were compared using the bandwidth factor of 0.5 and 1.0. The performance of the algorithm was significantly higher when using the bandwidth of 0.5 compared with that of 1 ($p < 0.05$).

On the other hand, the effect of duration of time window in which the features were calculated

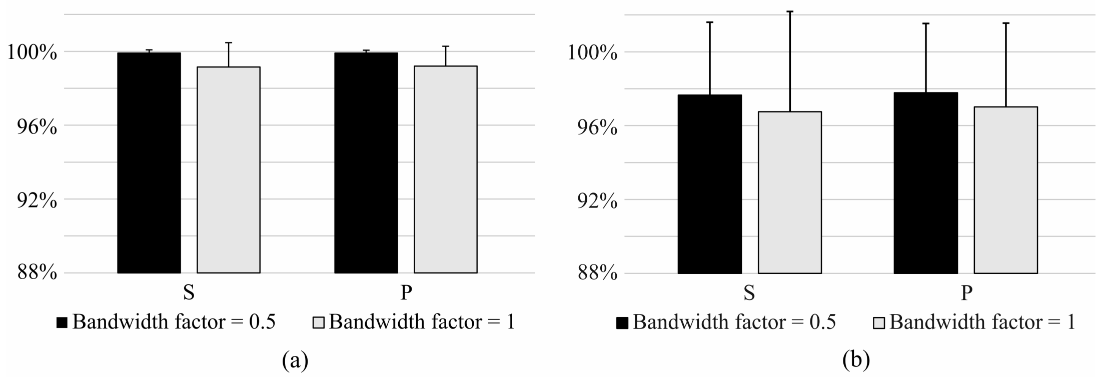

Figure 3.4: Sensitivity and precision of short-term identification of (a) identification of task and (b) identification of task and effort level using bandwidth factors 0.5 and 1.0 in mean shift algorithm.

was analyzed and results are presented in Figure 3.5. Identification based on the IMS features extracted from the 150 ms and 200 ms time windows significantly outperform the identification when features were extracted from shorter time windows, whereas no significant difference was found between results calculated on 150 ms and 200 ms windows.

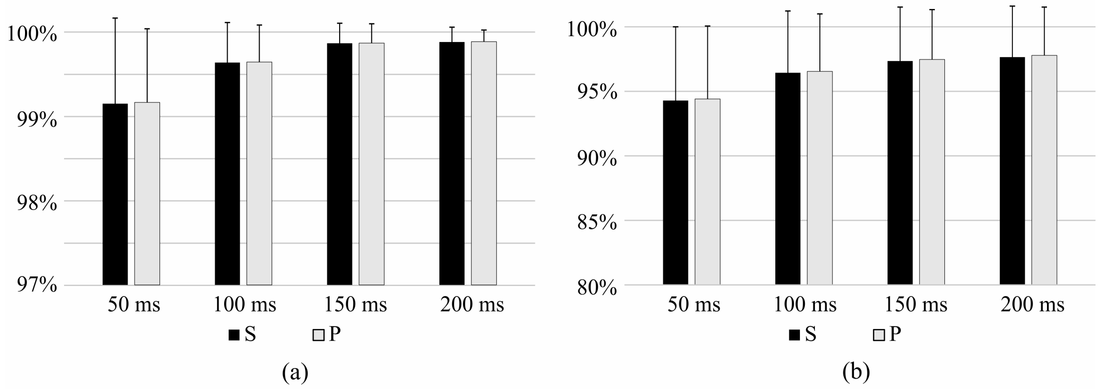

Figure 3.5: Sensitivity (S) and precision (P) of (a) identification of task and (b) identification of task and effort level for time windows of 50 ms, 100 ms, 150 ms, and 200 ms.

Consequently, the bandwidth factor of 0.5 and the time window of 150 ms were used in the rest of the paper.

3.3.2 Short-Term Identification

Table 3.1 shows the results of the identification of task using the novel features proposed in this paper and Figure 3.6 shows the comparison between IMS, ICG, I, TD, an Diff features in the identification of tasks. IMS significantly outperformed all of the compared features ($p < 0.05$).

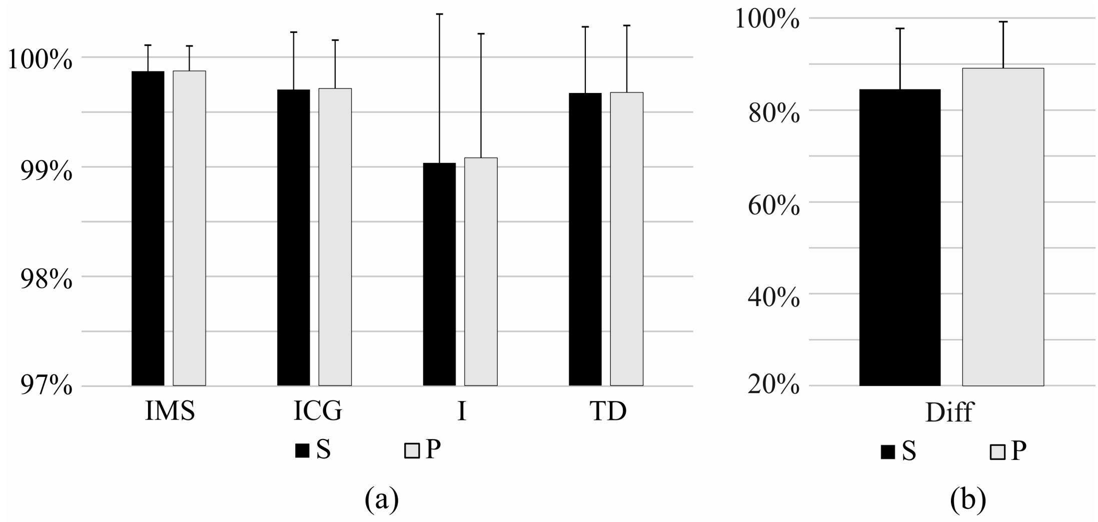

Figure 3.6: Sensitivity (S) and precision (P) of short-term identification of task using (a) IMS, ICG, I, and TD features, and (b) using Diff features. Results of the identification using Diff is showed in a different scale.

Table 3.1: Sensitivity and precision of identification of task using IMS features averaged between patients. Identification Indices for each patient were calculated as an average of hold-out repetitions ($N = 20$) and presented in terms of mean and standard deviation.

Task	Sensitivity%	Precision %
Flexion	99.7 ± 0.5	99.9 ± 0.2
Extension	99.9 ± 0.1	99.9 ± 0.1
Supination	99.9 ± 0.2	99.7 ± 0.5
Pronation	99.9 ± 0.1	99.9 ± 0.1
Average	**99.9 ± 0.2**	**99.9 ± 0.2**

The results of the identification of the task and effort level using IMS features are given in Table 3.2, whereas comparison between IMS and other features is shown in Figure 3.7. IMS features significantly outperform I, TD, and Diff features ($p < 0.05$), whereas the ICG features slightly outperform IMS features ($\Delta S = 0.6\%$, $\Delta P = 0.6\%$; $p < 0.05$).

The sensitivity and precision of the task identification when the classifier was trained using all effort levels (pool of 10%, 30%, 50% MVC) and tested using a specific effort level can be seen in Figure 3.8 and Figure 3.9 for comparison of IMS, ICG, I, and TD features, and for Diff features, respectively. This experiment shows how well each feature set identifies the task of a specific effort level. The difference in performance is especially pronounced in the identification of tasks at very low effort level (10% MVC). IMS significantly outperforms I and Diff features at all

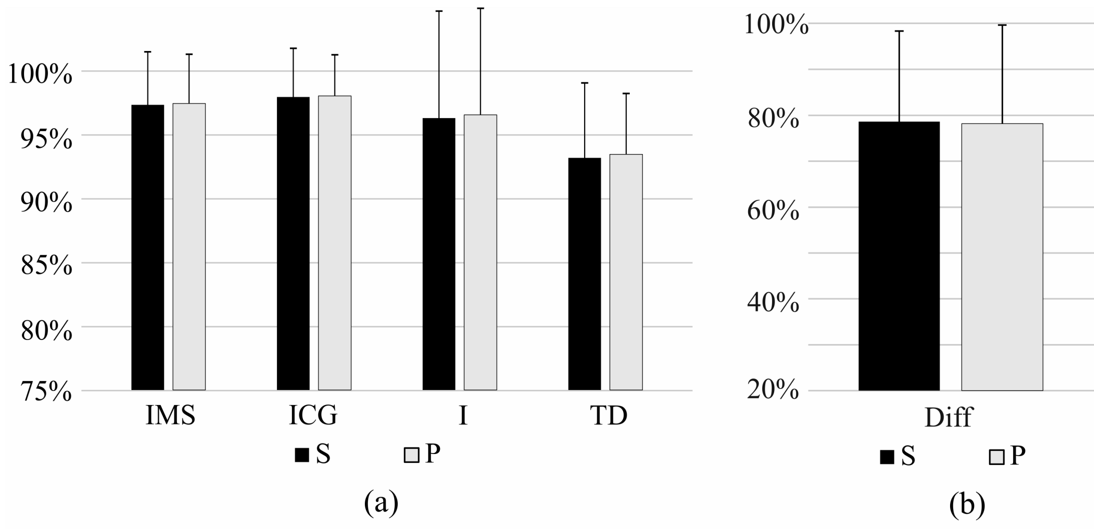

Figure 3.7: Sensitivity (S) and precision (P) of short-term identification of task and effort level using (a) IMS, ICG, I, and TD features, and (b) using Diff features. Results of the identification using Diff is showed in a different scale.

Table 3.2: Sensitivity and precision of identification of task and effort level averaged between patients. Identification indices for each patient were calculated as an average of hold-out repetitions (N = 20) and presented in terms of mean and standard deviation.

Task	Sensitivity%	Precision %
Flexion 10% MVC	98.2 ± 2.8	99.9 ± 0.3
Flexion 30% MVC	98.7 ± 1.1	97.0 ± 3.1
Flexion 50% MVC	97.7 ± 2.9	98.6 ± 1.1
Extension 10% MVC	99.7 ± 0.6	99.6 ± 1.1
Extension 30% MVC	97.4 ± 3.4	97.5 ± 2.1
Extension 50% MVC	97.7 ± 2.3	98.2 ± 2.9
Supination 10% MVC	99.7 ± 0.5	99.9 ± 0.2
Supination 30% MVC	95.2 ± 7.1	96.0 ± 5.1
Supination 50% MVC	96.6 ± 4.9	95.4 ± 6.3
Pronation 10% MVC	99.8 ± 0.2	99.4 ± 1.1
Pronation 30% MVC	93.8 ± 12.3	93.9 ± 11.3
Pronation 50% MVC	93.7 ± 11.9	94.2 ± 11.9
Average	**97.4 ± 4.2**	**97.5 ± 3.9**

effort levels, but the difference between IMS and ICG features and the difference between IMS and TD are not significant at moderate effort levels (30% MVC and 50% MVC), whereas IMS features are specifically and significantly better when identifying tasks at low effort levels (10% MVC).

Additionally, no significant difference between task identification at three different effort levels was seen when using IMS features, whereas these differences were significant for other feature sets. This could mean that these novel IMS features are more robust to the variation in the

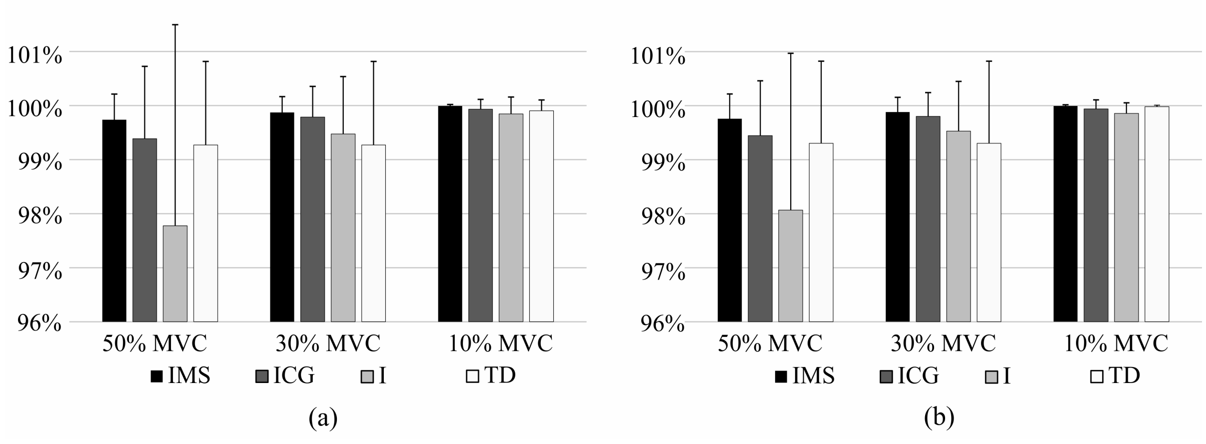

Figure 3.8: Figure shows sensitivity (a) and precision (b) of short-term identification of task recorded at specific effort level using IMS, ICG, I, and TD features.

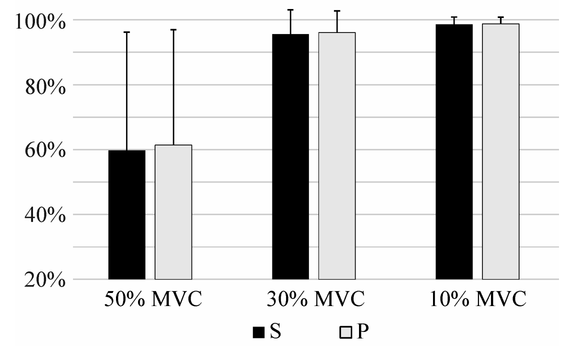

Figure 3.9: Figure shows sensitivity (S) and precision (P) of short-term identification of task recorded at specific effort level using Diff features.

effort level.

3.3.3 Long-Term Identification

Identification was tested when a significant amount of time passed between the recording of the training and test sets. This allowed an evaluation of influence of slow time-dependent changes in the EMG signal on the robustness of the identification. Figure 3.10 shows the comparison of the intensity features and the combination of intensity and spatial features when these last ones were calculated as the center of gravity or using the mean shift algorithm. There are no significant differences in performances between these IMS, ICG, and I features, whereas IMS feature significantly outperform TD and Diff features ($p < 0.05$). However, it should be noted that the test set was composed only of samples recorded at 50% MVC. And, as previously proven in literature (Jordanic et al., 2016), and shown in Figure 3.8 and Figure 3.9, the use of spatial information is particularly useful in contractions at low effort levels, whereas only intensity can be sufficient to successfully identify contractions of moderate effort levels (as 50% MVC).

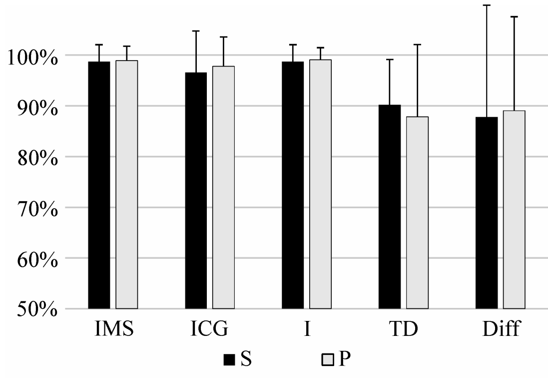

Figure 3.10: Sensitivity (S) and precision (P) of long-term identification of task using IMS, ICG, I, TD, and Diff features.

3.3.4 Identification During Fatigue

The influence of fatigue on EMG was evaluated using endurance recordings. Recordings were divided into five equal time epochs. The training set was obtained from the first epoch (0–20% TDR), and the identification was performed on all five time epochs. Changes of sensitivity and precision during the exercise can be seen in Figure 3.11. It can be seen how all feature sets perform similarly at the beginning of the contraction, whereas identification indices decay towards the end as the fatigue accumulates. However at the final stages of fatigue (80%–100% TDR) IMS features significantly outperform other feature sets ($p < 0.05$). These results show the robustness of the IMS features to the fatigue.

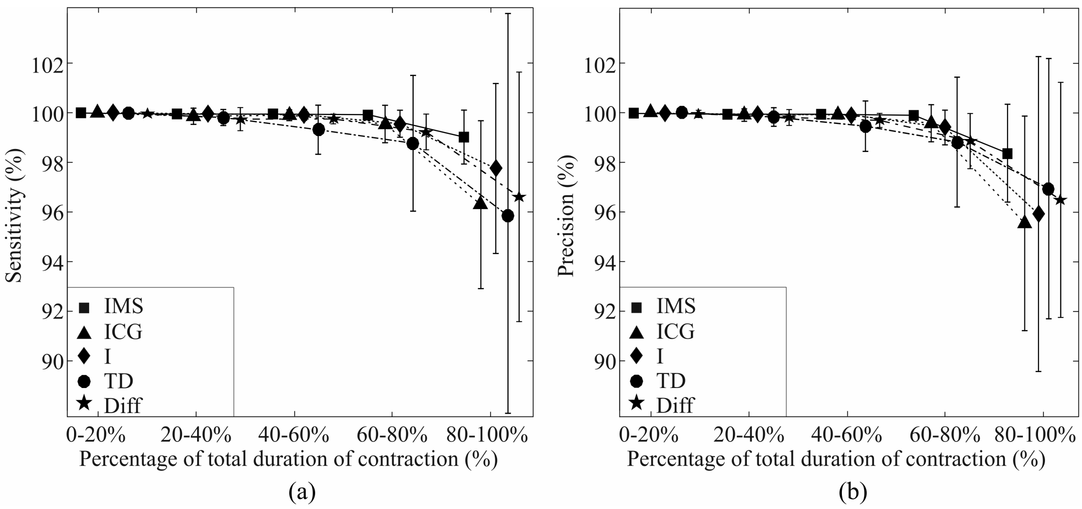

Figure 3.11: Influence of fatigue on (a) sensitivity and (b) precision of the identification of task using IMS, ICG, I, TD, and Diff features.

3.4 Discussion

This study showed that the combination of intensity and spatial information is useful for the extraction of neuromuscular information. The spatial information was calculated from the RMS activation maps using the mean shift algorithm. Results were evaluated using the 70% repeated holdout method and stratified sampling as to have sufficient number of samples of each class in the sets. To prevent the type III statistical error (Mosteller, 1948; Mohebian et al., 2017), a repeated hold-out was used. Sensitivity and precision, as appropriate unbiased measures in analyzing imbalanced multi-class problems (Jordanić et al., 2016; Rojas-Martínez et al., 2013), were used to quantify the identification.

IMS features achieved very good results compared to other feature sets during task identification when the task was performed at very low effort level. Moreover, the Friedman test showed no significant differences in task identification using IMS when tasks were performed at 10% MVC, 30% MVC, or 50% MVC. This can be a very important quality in everyday applications where subject could not need to contract muscles at moderate effort level to complete the task. It can be a step toward more natural control where even slight contractions can be successfully identified. In fact, only activations with low level of intensity are sometimes possible in patients with neuromuscular impairments.

A high identification rate is not the only factor important in the extraction of neural information from sEMG. The system should also be robust to slow time-dependent changes such as fatigue and electrode-skin contact impedance (Farina et al., 2014). Therefore, the robustness of the proposed features was tested with respect to time and fatigue. When evaluating the time effect, no significant differences in performance were found between IMS, ICG, and I feature sets and IMS significantly outperformed TD and Diff features. However, time effect was evaluated only when test set was composed of contractions recorded at 50% MVC and, as shown in Figure 3.6, all features perform similarly for the identification of that effort level. This phenomenon was already remarked and described in (Jordanic et al., 2016) where authors noted that adding spatial features to intensity features significantly improved the identification of tasks recorded at low effort levels, whereas improvement is not significant at moderate effort levels. On the other hand, the proposed features are particularly robust in task identification during fatiguing exercises and show significantly higher identification rate when compared to other features. Further improvements in reliability of the identification during the long-term contractions and fatiguing contractions can be achieved by using adaptive identification models that are being constantly updated during the usage (e.g., (Vidovic et al., 2016; Hahne et al., 2015; Sensinger et al., 2009)).

In the current work, features were extracted from the RMS activation maps of the HD-EMG. Although these features proved to be very effective, by describing the EMG signal with its RMS value, i.e., the estimator of variance, the information is partially lost. Since the gradient of the probability density function of raw EMG is a useful feature in task identification, statistical measures (e.g., modes) of the raw HD-EMG, i.e., joint distribution of instantaneous EMG amplitude over the electrode array, could provide valuable information. Moreover, in literature, features were often calculated for each channel separately and selected using the simple sequential method prior to classification (Hargrove et al., 2009; Li et al., 2017). On the other hand, Geng et al. recently proposed a more advanced channel selection method based on common spatial patterns (Geng et al., 2014). Modes of the HD-EMG density function could be correlated with the channels with discriminative information and could be a useful tool in channel selection.

Finally, the mean shift algorithm can be used for clustering and, since it was shown that the algorithm is most effective in low-dimensional data, image segmentation is one of its most successful applications (Comaniciu and Meer, 2002). A mode of the density estimate, or in this case, a channel selected by the mean shift algorithm, can be considered as a cluster representative (Hennig et al., 2015), related to the possible image segments, where spatial (pixel locations) and range features (the intensity of the grayscale value) are considered. The advantage of the mean shift is that it can be used for clustering non-convex shapes, albeit, it could segment complex non-convex regions in the activation maps. Since segmentation of the muscle activation map can improve the neuromuscular activity estimation (Vieira et al., 2010), this could be a reason why mean shift features improved the performance of the movement detection system compared with previously published attributes. In addition, the algorithm only requires setting one parameter, bandwidth (h) and, unlike in the similar methods, it is not necessary to define the number of expected clusters. This is a big advantage because it does not require a priori knowledge on the number of clusters.

As a limitation of the study, it should be noted that the proposed features were tested only in highly controlled conditions of isometric contractions. The experiments during non-isometric contractions should be performed in order to validate the quality of the features in dynamic and more natural movements. Also, the experiment included only four tasks related to the elbow joint. Further analysis should include higher number of more complex tasks related to hand and shoulder. Moreover, all results were obtained during offline analysis. To evaluate practical aspects of the features, the experiment should be repeated using online identification and considering multiple transitions between tasks.

3.5 Conclusions

In conclusion, a new set of features for the identification of isometric motor tasks of upper limb was proposed. It was based on the combination of intensity and the spatial distribution of intensity of HD-EMG. These new features were evaluated using the LDA classifier and the results showed they improve the identification of tasks. Moreover, robustness of the features was tested under the influence of slow time-dependent changes of the EMG. They proved to be particularly useful for task identification when muscles were fatigued. The proposed methods could be used for the design and monitoring of rehabilitation therapies intended for patients with neuromuscular impairment, as well as for the control of external devices like exoskeletons, and prostheses.

3.6 Acknowledgments

Special acknowledgement to Laboratory of Engineering of Neuromuscular System and Motor Rehabilitation at the Politecnico di Torino for the help and collaboration during the experiments. This work has been partially supported by the Spanish Ministry of Economy and Competitiveness (Project DPI2014-59049-R), People Programme (Marie Curie Actions) of the Seventh Framework Programme of the European Union (FP7/2007-2013) under REA grant agreement no. 600388 (TECNIO spring programme), and by the grant for the recruitment of early-stage research staff (FI 2014) from the AGAUR, Generalitat de Catalunya, Spain.

3.7 Author Contributions

M.R.-M. and M.A.M. conceived and designed the experimental protocol and conducted the experiments. M.J., M.R.M. and M.A.M. designed the study and interpreted the results. M.J. was in charge of the implementation of signal processing and machine learning methods and the analysis of the data. J.F.A. and H.R.M. aided in the analysis of the data and in the interpretation of results. M.J. wrote the manuscript and all authors contributed to the revising it.

3.8 Conflicts of Interest

The authors declare no conflict of interest.

3.9 Appendix A

The mean shift algorithm is a non-parametric approach to estimate the gradient of a density function. It was first proposed by Fukunaga and Hostetler (Fukunaga and Hostetler, 1975) in 1975, but did not get a lot of attention of the academic community initially. Although their work was cited more than 1500 times in literature, most of the cites occurred after the famous publication of Comaniciu and Meer (Comaniciu and Meer, 2002) in 2002 (counting almost 6000 citations) that revised the method and drew attention of the scientific community to it.

The algorithm is the enhanced version of the Parzen window technique for the estimation of density using a kernel (Parzen, 1962) and its extension to multivariate distributions (Cacoullos, 1966), given that density for the point $\mathbf{x}$ can be estimated based on the observed samples $\mathbf{x}_i$ $(i = 1, 2, \ldots, n)$ using the kernel function K as:

$$\hat{f}(\mathbf{x}) = \frac{1}{n} \sum_{i=1}^{n} K_H(\mathbf{x} - \mathbf{x}_i) \tag{3.7}$$

$$K_H = |\mathbf{H}|^{-\frac{1}{2}} K(\mathbf{H}^{-\frac{1}{2}} \mathbf{x}) \tag{3.8}$$

where $\hat{f}(\mathbf{x})$ is the estimated density, K_H is the normalized kernel function, and H is dxd bandwidth matrix. The bandwidth matrix H can be fully parameterized, diagonal, or, as in this paper, proportional to identity matrix ($\mathbf{H} = h\mathbf{I}$), which simplifies the expression for the density estimation to:

$$\hat{f}(\mathbf{x}) = \frac{1}{nh^d} \sum_{i=1}^{n} K(\frac{\mathbf{x} - \mathbf{x}_i}{h}) \tag{3.9}$$

where $\hat{f}(\mathbf{x})$ is the estimated density, h is a single bandwidth parameter, d is the number of dimensions, and K is the kernel function. Two commonly used univariate kernel profiles are Epanechnikov (k_E) and Gaussian (k_N):

$$k_N(x) = e^{-\frac{1}{2}x}, \ x \geq 0 \tag{3.10}$$

$$k_E(x) = \begin{cases} 1 - x & 0 \le x \le 1 \\ 0 & x > 1 \end{cases} \tag{3.11}$$

which yield multivariate radially symmetric kernel (K_E) and normal kernel (K_N) respectively:

$$K_N(\mathbf{x}) = \frac{1}{2\pi^{d/2}} e^{-\frac{1}{2}\|\mathbf{x}\|^2} \tag{3.12}$$

$$K_E(\mathbf{x}) = \begin{cases} \frac{1}{2}\frac{d+2}{c_d}\left(1 - \parallel \mathbf{x} \parallel^2\right) & \parallel \mathbf{x} \parallel \le 1 \\ 0 & \parallel \mathbf{x} \parallel > 1 \end{cases} \tag{3.13}$$

where d is the number of dimension and c_d is the constant that ensures the kernel integrates to one. Mean shift vector is defined as (Comaniciu and Meer, 2002):

$$\mathbf{ms}(\mathbf{x}) = \frac{\sum_{i=1}^{n} \mathbf{x}_i \, g(\parallel \frac{\mathbf{x}-\mathbf{x_i}}{h} \parallel^2)}{\sum_{i=1}^{n} g(\parallel \frac{\mathbf{x}-\mathbf{x}_i}{h} \parallel^2)} - \mathbf{x} \tag{3.14}$$

where $g(x)$ is the negative derivative of the original univariate kernel profile $k(x)$:

$$g(x) = -\frac{dk(x)}{dx} \tag{3.15}$$

Mean shift is a function defined for every point in space. It is a vector of difference between the current position and the weighted mean of all points within its bandwidth h, whose weights are defined by the kernel profile $g(x)$. Therefore, the mean shift vector always points to the direction of maximum increase of the density and can be considered as a function proportional to the gradient of the density function:

$$\mathbf{ms}_g(\mathbf{x}) \propto \nabla \hat{f}_k(\mathbf{x}) \tag{3.16}$$

In addition, mean shift can be effectively used to find modes (local maxima) of the underlying density function by an iterative procedure. Kernel is usually centered at a random point in space and the mean shift vector is calculated. In the next iteration, the kernel is centered at the location pointed by the mean shift vector. The procedure is mathematically defined as:

$$\mathbf{y}_{i+1} := \frac{\sum_{j=1}^{n} \mathbf{x}_j \, g(\| \frac{\mathbf{y}_i - \mathbf{x}_j}{h} \|^2)}{\sum_{j=1}^{n} g(\| \frac{\mathbf{y}_i - \mathbf{x}_j}{h} \|^2)} \tag{3.17}$$

By repeating this procedure, at every step, the center of the kernel is shifted to the direction of maximum increase of the density function until the local maximum is reached. At this location, the difference between two consecutive points is zero (up to a tolerance). These final stationary points are considered to be modes of the probability density function:

$$\mathbf{y}_{i+1} - \mathbf{y}_i = 0 \tag{3.18}$$

$$\mathbf{y}_{i+1} - \mathbf{y}_i = 0 \tag{3.19}$$

$$\mathbf{ms}_g(\mathbf{y}_i) = \nabla \hat{f}_k \, (\mathbf{y}_i) = 0 \tag{3.20}$$

This algorithm is very useful in image processing and feature space analysis with many applications, of which clustering is the most popular. It only requires setting one parameter, bandwidth (h). On the other hand, unlike the similar methods, e.g., $k-$ means clustering, it is not necessary to define the number of expected clusters. This is a big advantage because it does not require *a priori* knowledge on the number of clusters. Detailed explanation of the mean shift algorithm can be found in the literature (Comaniciu and Meer, 2002; Fukunaga and Hostetler, 1975).

In this study, modes of the density function of root-mean-square (RMS) activation maps were found using the mean shift algorithm implemented in Python (Pedregosa et al., 2011) and were used as features in the identification. The Epanechnikov kernel profile was employed to describe the density function, which yielded flat kernel profile $g(x)$ in the calculation of the mean shift vector:

$$g(x) = \begin{cases} 1, & \| x \| \leq h \\ 0, & \| x \| > h \end{cases} \tag{3.21}$$

This choice of the kernel profile simplified the update of the mean shift centroid to:

$$\mathbf{y}_{i+1} := \frac{\sum_{j=1}^{N} \mathbf{x}_j}{N} \Bigg|_{\forall \mathbf{x}\, s.t.\, \|\mathbf{x}-\mathbf{y}_i\| \leq h} \tag{3.22}$$

In the other words, the new centroid was calculated as the mean value of N points located within the Euclidean distance h from the current centroid.

3.10 Appendix B

Example of the torque signals during supination and pronation can be seen in the Figure 3.12, along with the EMG signal recorded on pronator teres. It is possible to observe that the polarity of the torque signals change depending on the direction of the movement. The mechanical brace is fixed at the wrist so that the exerted force during supination and pronation is monitored by left and right torque meters, respectively. In addition, as expected, the amplitude of the sEMG signal in the Pronator Teres is higher during pronation.

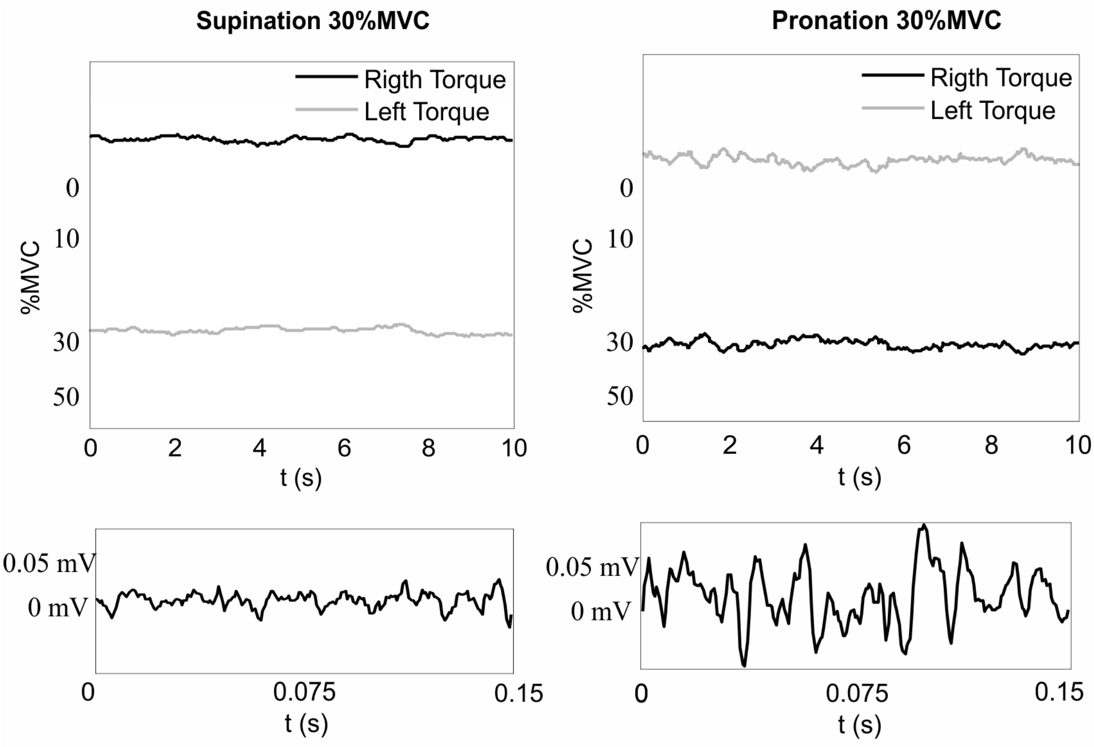

Figure 3.12: Example of torque and EMG signals in supination and pronation in one subject. Left. Supination at 30% MVC. The exerted torque on right (black) and left (gray) sides of the mechanical brace are shown at the top of the figure. The sEMG signal recorded on one of the channels of the Pronator Teres muscle is shown at the bottom. Rigth. Torque signals for Pronation at 30% MVC are shown on the top of the figure. The sEMG signal recorded on the same channel as in the previous case is shown at the bottom.

On the other hand, examples of EMG signals recorded on five muscles during 30% MVC flexion, extension, supination, and pronation can be seen in Figure 3.13, Figure 3.14, Figure 3.15 and Figure 3.16, respectively. Figures show raw EMG signals and signals filtered using 4$^{\text{th}}$ order Butterworth filter with cut-off frequencies of of 15 Hz and 350 Hz. Scale for each muscle is the same across different tasks to show difference in EMG amplitudes in dependence of task.

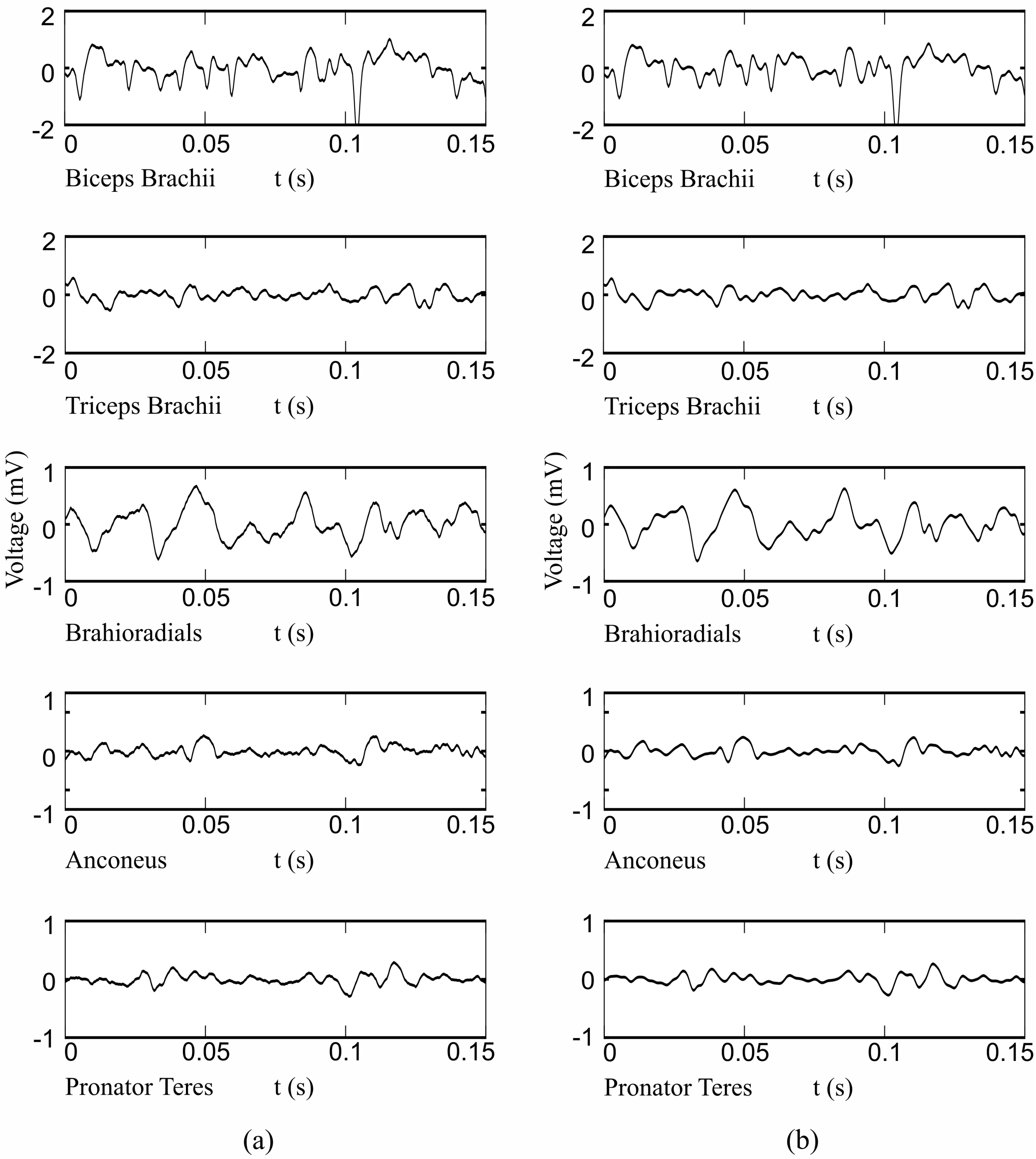

Figure 3.13: Examples of recorded EMG signals from five muscles (biceps brachii, triceps brachi, brachioradialis, anconeus, bracioradialis, and pronator teres) during flexion. Figure shows (a) raw signals and (b) signals filtered using 4^{th} order Butterworth filter with the cut-off frequencies of 15 Hz and 350 Hz.

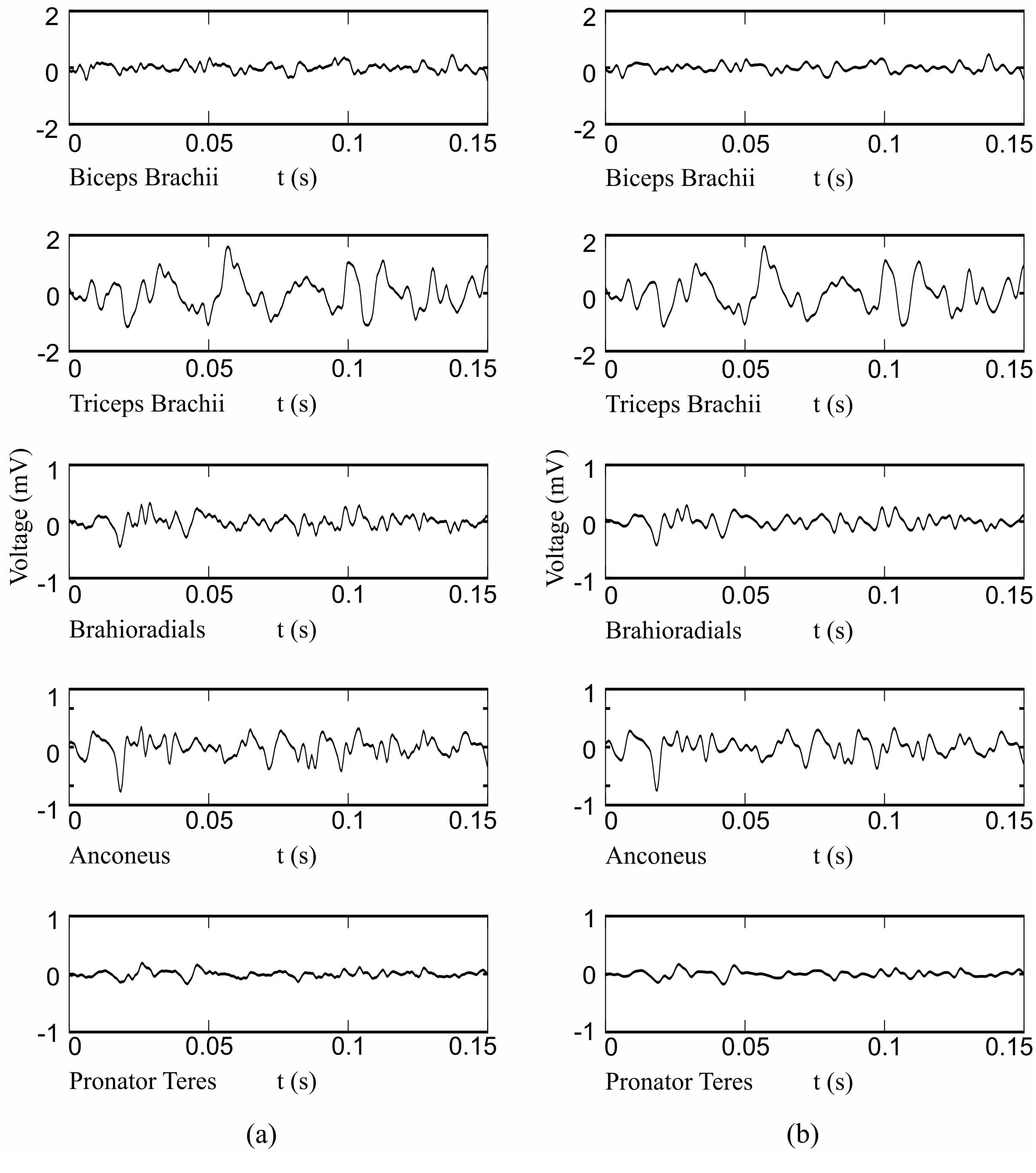

Figure 3.14: Example of recorded EMG signals from five muscles (biceps brachii, triceps brachi, brachioradialis, anconeus, bracioradialis, and pronator teres) during extension. Figure shows (a) raw signals and (b) signals filtered using 4th order Butterworth filter with the cut-off frequencies of 15 Hz and 350 Hz.

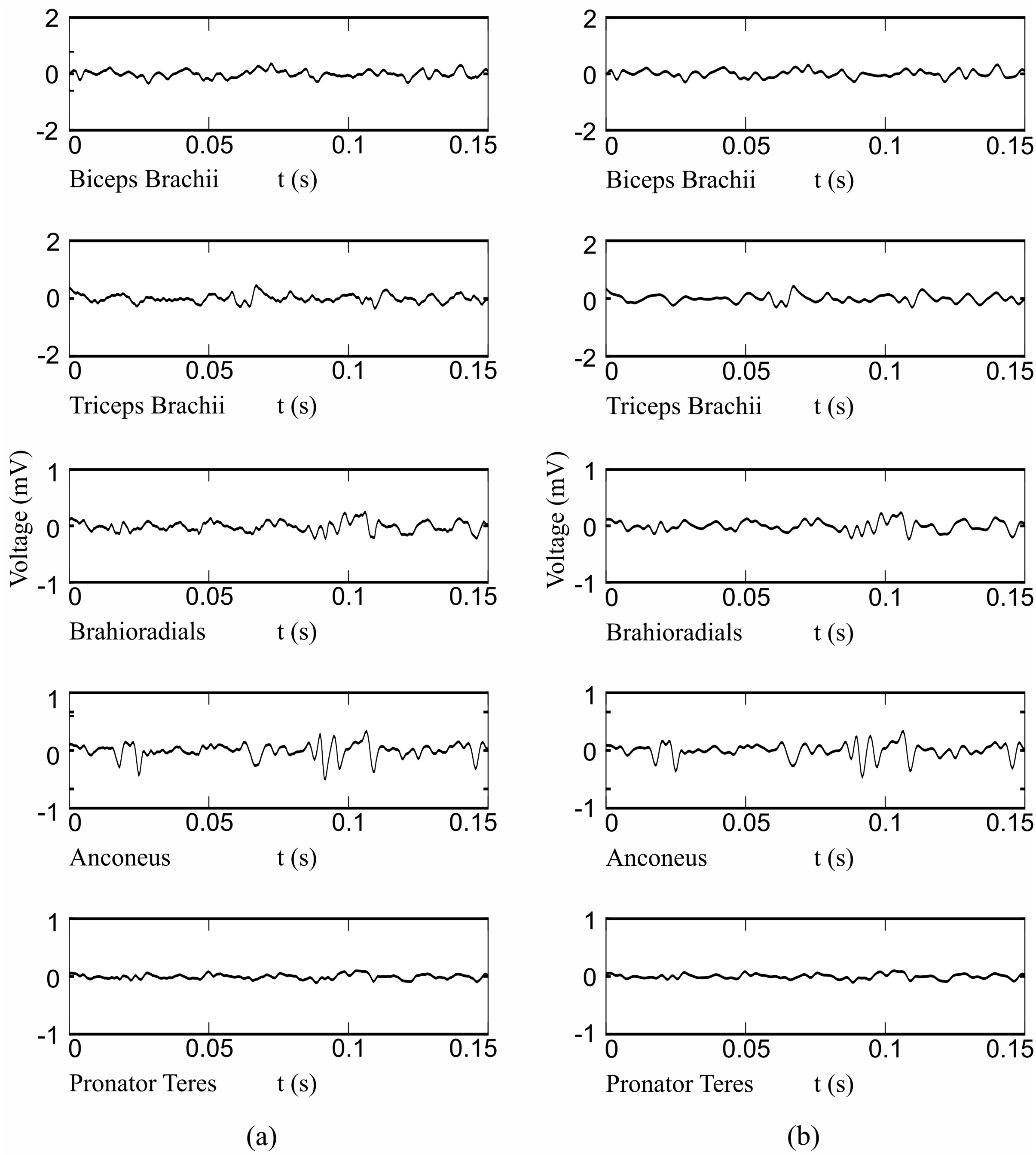

Figure 3.15: Example of recorded EMG signals from five muscles (biceps brachii, triceps brachi, brachioradialis, anconeus, bracioradialis, and pronator teres) during supination. Figure shows (a) raw signals and (b) signals filtered using 4^{th} order Butterworth filter with the cut-off frequencies of 15 Hz and 350 Hz.

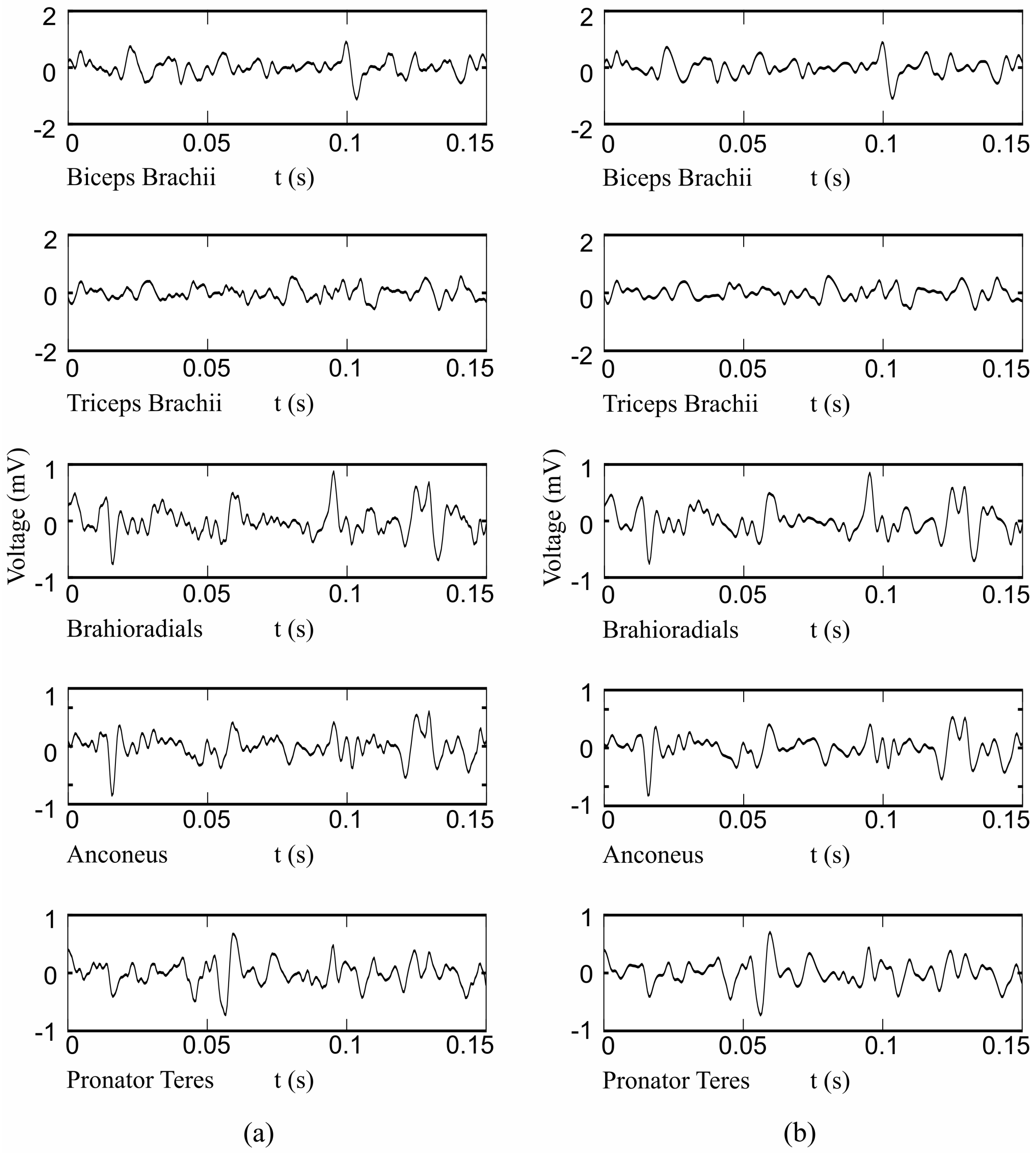

Figure 3.16: Example of recorded EMG signals from five muscles (biceps brachii, triceps brachi, brachioradialis, anconeus, bracioradialis, and pronator teres) during pronation. Figure shows (a) raw signals and (b) signals filtered using 4^{th} order Butterworth filter with the cut-off frequencies of 15 Hz and 350 Hz.

Notes

Bibliography

MATLAB and Statistics and Machine Learning Toolbox Release 2015a.

Ameri, A., Englehart, K. B., and Parker, P. a. A comparison between force and position control strategies in myoelectric prostheses. *Proceedings of the Annual International Conference of the IEEE Engineering in Medicine and Biology Society, EMBS*, pages 1342–1345, 2012.

Boschmann, A. and Platzner, M. Reducing the Limb Position Effect in Pattern Recognition Based Myoelectric Control using a High Density Electrode Array. *2013 ISSNIP Biosignals and Biorobotics Conference (BRC)*, pages 1–5, 2013.

Cacoullos, T. Estimation of a multivariate density. *Annals of the Institute of Statistical Mathematics*, 18(1):179–189, 1966.

Celadon, N., Došen, S., Binder, I., Ariano, P., and Farina, D. Proportional estimation of finger movements from high-density surface electromyography. *Journal of NeuroEngineering and Rehabilitation*, 2016.

Comaniciu, D. and Meer, P. Mean shift: a robust approach toward feature space analysis. *IEEE Transactions on Pattern Analysis and Machine Intelligence*, 24(5):603–619, 2002.

De Luca, C. J. Myoelectrical manifestations of localized muscular fatigue in humans. *Critical Reviews in Biomedical Engineering*, 11(4):251–79, jan 1984.

De Luca, C. J. The use of surface electromyography in biomechanics. *Journal of Applied Biomechanics*, 13(2):135–163, 1997.

Dipietro, L., Ferraro, M., Palazzolo, J. J., Krebs, H. I., Volpe, B. T., and Hogan, N. Customized interactive robotic treatment for stroke: EMG-triggered therapy. *IEEE Transactions on Neural Systems and Rehabilitation Engineering*, 13(3):325–334, 2005.

Du, Y., Jin, W., Wei, W., Hu, Y., and Geng, W. Surface EMG-Based Inter-Session Gesture Recognition Enhanced by Deep Domain Adaptation. *Sensors*, 17(3):458, 2017.

Farina, D., Colombo, R., Merletti, R., and Olsen, H. B. Evaluation of intra-muscular EMG signal decomposition algorithms. *Journal of Electromyography and Kinesiology*, 11(3):175–187, 2001.

Farina, D., Holobar, A., Merletti, R., and Enoka, R. M. Decoding the neural drive to muscles from the surface electromyogram. *Clinical Neurophysiology*, 121(10):1616–1623, 2010.

Farina, D., Jiang, N., Rehbaum, H., Holobar, A., Graimann, B., Dietl, H., and Aszmann, O. C. The extraction of neural information from the surface EMG for the control of upper-limb prostheses: emerging avenues and challenges. *IEEE Transactions on Neural Systems and Rehabilitation Engineering*, 22(4):797–809, jul 2014.

Fukunaga, K. and Hostetler, L. The estimation of the gradient of a density function, with applications in pattern recognition. *IEEE Transactions on Information Theory*, 21(1):32–40, 1975.

Geng, W., Du, Y., Jin, W., Wei, W., Hu, Y., and Li, J. Gesture recognition by instantaneous surface EMG images. *Scientific Reports*, 6(1):36571, 2016.

Geng, Y., Zhang, X., Zhang, Y.-T., and Li, G. A novel channel selection method for multiple motion classification using high-density electromyography. *Biomedical Engineering Online*, 13:102, 2014.

Greenhouse, S. W. and Geisser, S. On methods in the analysis of profile data. *Psychometrika*, 24(2):95–112, 1959.

Grouven, U., Bergel, F., and Schultz, A. Implementation of linear and quadratic discriminant analysis incorporating costs of misclassification. *Computer Methods and Programs in Biomedicine*, 49(1):55–60, jan 1996.

Hahne, J. M., Graimann, B., and Muller, K. R. Spatial filtering for robust myoelectric control. *IEEE Transactions on Biomedical Engineering*, 59(5):1436–1443, 2012.

Hahne, J. M., Dähne, S., Hwang, H. J., Müller, K. R., and Parra, L. C. Concurrent Adaptation of Human and Machine Improves Simultaneous and Proportional Myoelectric Control. *IEEE Transactions on Neural Systems and Rehabilitation Engineering*, 23(4):618–627, 2015.

Hakonen, M., Piitulainen, H., and Visala, A. Current state of digital signal processing in myoelectric interfaces and related applications. *Biomedical Signal Processing and Control*, 18: 334–359, 2015.

Hargrove, L., Li, G., Englehart, K., and Hudgins, B. Principal Components Analysis Preprocessing for Improved Classification Accuracies in Pattern-Recognition-Based Myoelectric Control. *IEEE Transactions on Biomedical Engineering*, 56(5):1407–1414, 2009.

Hargrove, L. J., Englehart, K., and Hudgins, B. A comparison of surface and intramuscular myoelectric signal classification. *IEEE Transactions on Biomedical Engineering*, 54(5):847–853, 2007.

He, J., Zhang, D., Sheng, X., Li, S., and Zhu, X. Invariant surface EMG feature against varying contraction level for myoelectric control based on muscle coordination. *IEEE Journal of Biomedical and Health Informatics*, 19(3):874–882, 2015.

Hennig, C., Meila, M., Murtagh, F., and Rocci, R. *Handbook of Cluster Analysis.* CRC Press, 2015.

Hermens, H. and Freriks, B. *SENIAM 9: European Recommendations for Surface ElectroMyoGraphy, results of the SENIAM project (CD).* Roessingh Research and Development, 1999.

Hogan, N., Krebs, H. I., Rohrer, B., Palazzolo, J. J., Dipietro, L., Fasoli, S. E., Stein, J., Hughes, R., Frontera, W. R., Lynch, D., and Volpe, B. T. Motions or muscles? Some behavioral factors underlying robotic assistance of motor recovery. *Journal of Rehabilitation Research and Development*, 43(5):605–618, 2006.

Holobar, A., Minetto, M. A., Botter, A., Negro, F., and Farina, D. Experimental Analysis of Accuracy in the Identification of Motor Unit Spike Trains From High-Density Surface EMG. *IEEE Transactions on Neural Systems and Rehabilitation Engineering*, 18(3):221–229, 2010.

Holtermann, A., Roeleveld, K., and Karlsson, J. S. Inhomogeneities in muscle activation reveal motor unit recruitment. *Journal of Electromyography and Kinesiology*, 15(2):131–137, apr 2005.

Huang, H., Zhou, P., Li, G., and Kuiken, T. Spatial filtering improves EMG classification accuracy following targeted muscle reinnervation. *Annals of biomedical engineering*, 37(9): 1849–57, 2009.

Huang, Y., Englehart, K. B., Hudgins, B., and Chan, A. D. C. A Gaussian mixture model based classification scheme for myoelectric control of powered upper limb prostheses. *IEEE Transactions on Biomedical Engineering*, 52(11):1801–1811, 2005.

Jordanic, M., Rojas-Martínez, M., Mañanas, M. A., and Alonso, J. F. Spatial distribution of HD-EMG improves identification of task and force in patients with incomplete spinal cord injury. *Journal of NeuroEngineering and Rehabilitation*, 13(1):41, 2016.

Jordanić, M., Rojas-Martínez, M., Mañanas, M. A., and Alonso, J. F. Prediction of isometric motor tasks and effort levels based on high-density EMG in patients with incomplete spinal cord injury. *Journal of Neural Engineering*, 13(4):046002, 2016.

Kendall, F. P., Kendall McCreary, E., and Provance, P. G. *Muscles: testing and function*. Williams & Wilkins, New York, 4 edition, 1993.

Landa, S. and Everitt, B. S. *A Handbook of Statistical Analyses using SPSS*. Chapman & Hall/CRC, Boca Raton, 2004.

Li, G., Schultz, A. E., and Kuiken, T. A. Quantifying pattern recognition- based myoelectric control of multifunctional transradial prostheses. *IEEE Transactions on Neural Systems and Rehabilitation Engineering*, 18(2):185–192, 2010.

Li, X., Samuel, O. W., Zhang, X., Wang, H., Fang, P., and Li, G. A motion-classification strategy based on sEMG-EEG signal combination for upper-limb amputees. *Journal of NeuroEngineering and Rehabilitation*, 14(1):2, 2017.

Li, Y., Chen, X., Zhang, X., and Zhou, P. Several practical issues toward implementing myoelectric pattern recognition for stroke rehabilitation. *Medical Engineering and Physics*, 36(6): 754–760, 2014.

Li, Z., Wang, B., Yang, C., Xie, Q., and Su, C. Y. Boosting-based EMG patterns classification scheme for robustness enhancement. *IEEE Journal of Biomedical and Health Informatics*, 2013.

Liu, J. and Zhou, P. A novel myoelectric pattern recognition strategy for hand function restoration after incomplete cervical spinal cord injury. *IEEE Transactions on Neural Systems and Rehabilitation Engineering*, 21(1):96–103, 2013.

Liu, J., Sheng, X., Zhang, D., Jiang, N., and Zhu, X. Towards Zero Retraining for Myoelectric Control Based on Common Model Component Analysis. *IEEE Transactions on Neural Systems and Rehabilitation Engineering*, 24(4):444–454, 2016.

Loftus, G. R. and Masson, M. E. Using confidence intervals in within-subject designs. *Psychonomic bulletin & review*, 1(4):476–90, 1994.

Mañanas, M., Romero, S., Topor, Z., Bruce, E., Houtz, P., and Caminal, P. Cardiac interference in myographic signals from different respiratory muscles and levels of activity. *2001 Conference Proceedings of the 23rd Annual International Conference of the IEEE Engineering in Medicine and Biology Society*, 2:1115–1118, 2001.

Marateb, H. R., McGill, K. C., and Webster, J. G. Electromyographic (Emg) Decomposition. In *Wiley Encyclopedia of Electrical and Electronics Engineering*. John Wiley & Sons, Inc, 1999.

Marateb, H. R., Farahi, M., Rojas, M., Mañanas, M. A., Farina, D., and Rix, H. Detection of Multiple Innervation Zones from Multi-Channel Surface EMG Recordings with Low Signal-to-Noise Ratio Using Graph-Cut Segmentation. *PLOS ONE*, 11(12), 2016.

Marchal-Crespo, L. and Reinkensmeyer, D. J. Review of control strategies for robotic movement training after neurologic injury. *Journal of Neuroengineering and Rehabilitation*, 6:20, 2009.

Merletti, R. and Hermens, H. Detection and Conditioning of the surface EMG signal. In *Electromyography: Physiology, Engineering, and Noninvasive Applications*, chapter 5, pages 115–120. Wiley, New Jersey, USA, 2004.

Merletti, R., Botter, A., Troiano, A., Merlo, E., and Minetto, M. A. Technology and instrumentation for detection and conditioning of the surface electromyographic signal: State of the art. *Clinical Biomechanics*, 24(2):122–134, 2009.

Mohebian, M. R., Marateb, H. R., Mansourian, M., Mañanas, M. A., and Mokarian, F. A Hybrid Computer-aided-diagnosis System for Prediction of Breast Cancer Recurrence (HPBCR) Using Optimized Ensemble Learning. *Computational and Structural Biotechnology Journal*, 15:75–85, 2017.

Mosteller, F. A k-Sample Slippage Test for an Extreme Population on JSTOR. *The Annals of Mathematical Statistics*, 19(1):58–65, 1948.

Muller-Putz, G., Leeb, R., Tangermann, M., Hohne, J. H., Kubler, A. K., Cincotti, F., Mattia, D., Rupp, R., Muller, K. R., and Millan, J. D. R. Towards Noninvasive Hybrid Brain–Computer Interfaces: Framework, Practice, Clinical Application, and Beyond. *Proceedings of the IEEE*, 103(6):926 – 943, 2015.

Nazmi, N., Abdul Rahman, M., Yamamoto, S.-I., Ahmad, S., Zamzuri, H., and Mazlan, S. A Review of Classification Techniques of EMG Signals during Isotonic and Isometric Contractions. *Sensors*, 16(8):1304, 2016.

Oskoei, M. A. and Hu, H. GA-based feature subset selection for myoelectric classification. *2006 IEEE International Conference on Robotics and Biomimetics, ROBIO 2006*, pages 1465–1470, 2006.

Oskoei, M. A. and Hu, H. Myoelectric control systems-A survey. *Biomedical Signal Processing and Control*, 2(4):275–294, 2007.

Parker, P., Englehart, K., and Hudgins, B. Myoelectric signal processing for control of powered limb prostheses. *Journal of Electromyography and Kinesiology*, 16:541–548, 2006.

Parzen, E. On Estimation of a Probability Density Function and Mode. *The Annals of Mathematical Statistics*, 33(3):1065–1076, 1962.

Pedregosa, F., Varoquaux, G., Gramfort, A., Michel, V., Thirion, B., Grisel, O., Blondel, M., Prettenhofer, P., Weiss, R., Dubourg, V., Vanderplas, J., Passos, A., Cournapeau, D., Brucher, M., Perrot, M., and Duchesnay, E. Scikit-learn: Machine Learning in Python. *Journal of Machine Learning Research*, 12:2825–2830, 2011.

Pizzigalli, L., Ahmaidi, S., and Rainoldi, A. Effects of sedentary condition and longterm physical activity on postural balance and strength responses in elderly subjects. *Sport Sciences for Health*, 10(2):135–141, 2014.

Rohm, M., Schneiders, M., Müller, C., Kreilinger, A., Kaiser, V., Müller-Putz, G. R., and Rupp, R. Hybrid brain-computer interfaces and hybrid neuroprostheses for restoration of upper limb functions in individuals with high-level spinal cord injury. *Artificial Intelligence in Medicine*, 59(2):133–142, 2013.

Rojas-Martínez, M., Mañanas, M. a., and Alonso, J. F. High-density surface EMG maps from upper-arm and forearm muscles. *Journal of Neuroengineering and Rehabilitation*, 9:85, jan 2012.

Rojas-Martínez, M., Mañanas, M. a., Alonso, J. F., and Merletti, R. Identification of isometric contractions based on High Density EMG maps. *Journal of Electromyography and Kinesiology*, 23(1):33–42, 2013.

Scheme, E. and Englehart, K. Training strategies for mitigating the effect of proportional control on classification in pattern recognition-based myoelectric control. *Journal of Prosthetics and Orthotics*, 25(2):76–83, 2013.

Searle, A. and Kirkup, L. A direct comparison of wet, dry and insulating bioelectric recording electrodes. *Physiological Measurement*, 21(2):271–83, 2000.

Sensinger, J., Lock, B., and Kuiken, T. Adaptive Pattern Recognition of Myoelectric Signals: Exploration of Conceptual Framework and Practical Algorithms. *IEEE Transactions on Neural Systems and Rehabilitation Engineering*, 17(3):270–278, 2009.

Stango, A., Negro, F., and Farina, D. Spatial Correlation of High Density EMG Signals Provides Features Robust to Electrode Number and Shift in Pattern Recognition for Myocontrol. *IEEE Transactions on Neural Systems and Rehabilitation Engineering*, 23(2):189–198, 2015.

Staudenmann, D., Roeleveld, K., Stegeman, D. F., and van Dieen, J. H. Methodological aspects of SEMG recordings for force estimation - A tutorial and review. *Journal of Electromyography and Kinesiology*, 20(3):375–387, 2010.

Staudenmann, D., van Dieën, J. H., Stegeman, D. F., and Enoka, R. M. Increase in heterogeneity of biceps brachii activation during isometric submaximal fatiguing contractions: a multichannel surface EMG study. *Journal of neurophysiology*, 111(5):984–90, 2014.

Tkach, D., Huang, H., and Kuiken, T. a. Study of stability of time-domain features for electromyographic pattern recognition. *Journal of Neuroengineering and Rehabilitation*, 7:21, 2010.

Tucker, K., Falla, D., Graven-Nielsen, T., and Farina, D. Electromyographic mapping of the erector spinae muscle with varying load and during sustained contraction. *Journal of Electromyography and Kinesiology*, 19(3):373–9, jun 2009.

Vaca Benitez, L. M., Tabie, M., Will, N., Schmidt, S., Jordan, M., and Kirchner, E. A. Exoskeleton technology in rehabilitation: Towards an EMG-based orthosis system for upper limb neuromotor rehabilitation. *Journal of Robotics*, 2013:13, 2013.

Valle, S., Li, W., and Qin, S. J. Selection of the Number of Principal Components: The Variance of the Reconstruction Error Criterion with a Comparison to Other Methods. *Industrial and Engineering Chemistry Research*, 38(11):4389–4401, 1999.

van Dijk, L., van der Sluis, C. K., van Dijk, H. W., Bongers, R. M., and Scheidt, R. Learning an EMG Controlled Game: Task-Specific Adaptations and Transfer. *PLOS ONE*, 11(8): e0160817, 2016.

Verikas, A., Vaiciukynas, E., Gelzinis, A., Parker, J., and Olsson, M. Electromyographic Patterns during Golf Swing: Activation Sequence Profiling and Prediction of Shot Effectiveness. *Sensors*, 16(5):592, 2016.

Vidovic, M. M.-C., Hwang, H.-J., Amsuss, S., Hahne, J. M., Farina, D., and Muller, K.-R. Improving the Robustness of Myoelectric Pattern Recognition for Upper Limb Prostheses by Covariate Shift Adaptation. *IEEE Transactions on Neural Systems and Rehabilitation Engineering*, 24(9):961–970, 2016.

Vieira, T. M. M., Merletti, R., and Mesin, L. Automatic segmentation of surface EMG images: Improving the estimation of neuromuscular activity. *Journal of Biomechanics*, 43(11):2149–58, 2010.

Wan, B., Xu, L., Ren, Y., Wang, L., Qiu, S., Liu, X., Liu, X., Qi, H., Ming, D., and Wang, W. Study on fatigue feature from forearm SEMG signal based on wavelet analysis. *2010 IEEE International Conference on Robotics and Biomimetics, ROBIO 2010*, pages 1229–1232, 2010.

Wang, Y., Li, J., and Li, Y. Measure for data partitioning in m x 2 cross-validation. *Pattern Recognition Letters*, 65:211–217, 2015.

Young, A. J., Hargrove, L. J., and Kuiken, T. a. Improving myoelectric pattern recognition robustness to electrode shift by changing interelectrode distance and electrode configuration. *IEEE Transactions on Biomedical Engineering*, 59(3):645–652, 2012.

Young, A. J., Smith, L. H., Rouse, E. J., and Hargrove, L. J. Classification of simultaneous movements using surface EMG pattern recognition. *IEEE Transactions on Biomedical Engineering*, 60(5):1250–1258, 2013.

Young, W. Spinal Cord Injury Levels & Classification, W M Keck Center for Collaborative Neuroscience.

Zhang, X. and Zhou, P. High-Density Myoelectric Pattern Recognition Toward Improved Stroke Rehabilitation. *IEEE Transactions on Biomedical Engineering*, 59(6):1649–1657, 2012.

Zimmer, C. and Sahle, S. Comparison of approaches for parameter estimation on stochastic models: Generic least squares versus specialized approaches. *Computational Biology and Chemistry*, 61:75–85, 2016.